



Time-Frequency-Based Data-Driven Structural Diagnosis and Damage Detection for Cable-Stayed Bridges

Hong Pan¹; Mohsen Azimi²; Fei Yan³; and Zhibin Lin, M.ASCE⁴

Abstract: Dynamic characteristics of cable-stayed bridges are widely accepted as valuable indicators to determine their performance in structural health monitoring (SHM). Although research has been extensively conducted in this area, such vibration-based physics methods still face great challenges in improving the effectiveness of damage identification from complex large-scale systems, particularly when other factors, including operational and environmental conditions, may cause high interference to the vibration response. Data-intensive machine learning techniques have been gaining attention due to their robustness for data classification. In this study, a framework was developed for data-driven structural diagnosis and damage detection using a support vector machine (SVM) integrated with enhanced feature extraction techniques for rapid condition assessment for large-scale cable-stayed bridges. The wavelet transform, Hilbert-Huang transform (HHT), and Teager-Huang transform (THT) were selected as three representative feature extraction methods. A kernel function-based SVM was used to facilitate the identification of damaged and undamaged cases. Numerical simulation was conducted to verify the effectiveness and accuracy of the proposed methods applied to a cable-stayed bridge. Results showed that the wavelet time-frequency analysis is more robust to noise than the HHT and THT, whereas the latter two transforms are more sensitive to capture damage/defects. Moreover, for regular signal data, the THT, due to the high time resolution, had the highest concentration and thus is the most sensitive compared with the other two methods. Parameters of interest, including impacts of damage level, damage location, sensor locations, and moving vehicle loading, are extensively discussed. All cases reveal that data-driven approaches could effectively map damage features over and under undamaged cases, dramatically enhancing the effectiveness and accuracy of data classification, which will greatly benefit in situ cable-stayed bridge assessment and management. DOI: [10.1061/\(ASCE\)BE.1943-5592.0001199](https://doi.org/10.1061/(ASCE)BE.1943-5592.0001199). © 2018 American Society of Civil Engineers.

Author keywords: Cable-stayed bridge; Data driven; Structural health monitoring (SHM); Machine learning; Damage detection.

Introduction

An ever-increasing amount of cable-stayed bridges have been constructed in the United States and other countries in recent decades. Cable-stayed bridges are robust and competitive systems for long-span crossings over conventional bridges. The stay cable, anchorage, bridge deck, and pylon are the major components in a cable-stayed bridge and are used to maintain structural integrity under in-service operational stages or any extreme events. Such long-span bridges, however, are vulnerable to fatigue-induced damage and environmental attacks. Particularly, aging effects, climate change, and ever-increasing traffic conditions (volume, size, and weight) accelerate the deterioration of the bridges. As recently reported (Li

and Ou 2016), the cable-stayed bridges have exhibited certain levels of structural degradation, including tension loss in cables, steel corrosion, degradation of anchorage, and deck fatigue and fractures (Yan et al. 2016; Yan et al. 2017). For instance, in recent years, fatigue-prone cracks in many cable-stayed orthotropic bridge decks have been reported in the United States (Fasl 2013), Europe (Maljaars et al. 2012), China (Ge and Xiang 2011; Guo et al. 2015; Xia et al. 2013), and other countries (Battista et al. 2008).

Dynamic characteristics of large-scale cable-stayed bridges could yield valuable information regarding their performance. To effectively capture abnormally dynamic characteristics of such long-span bridges while avoiding catastrophic failures, various strategies using sensors have been widely accepted in structural health monitoring (SHM). Among many sensor technologies, use of wireless sensor networks can overcome the limitations of the traditional power-wire-based sensor systems to facilitate SHM and detect potential damage (Ge et al. 2016; Herrasti et al. 2016; Huang et al. 2015; Pan et al. 2016; Watters et al. 2002; Worden et al. 2007), including favorable features of wireless data transmission, high reliability, and ease of operation. Particularly, integration of wireless sensor networks with unmanned aerial systems (UAS) technology has recently demonstrated great potential for SHM of the large-scale civil infrastructures (Ge et al. 2016; Pan et al. 2016). These advanced sensor technologies enable engineers to capture large amounts of data. The complexity and heterogeneity of these sensor data, however, pose great challenges to big data analysis for SHM and damage detection (Pan et al. 2016; Gui et al. 2017).

Much research has been conducted on data analysis using physics-based approaches (Salawu 1997; Doebling et al. 1998;

¹Ph.D. Student, School of Architecture and Civil Engineering, Jinggangshan Univ., Ji'an, Jiangxi 343009, China.; Ph.D. Student, School of Civil Engineering, Tongji Univ., Shanghai 200092, China.; Visiting Ph.D. Student, Dept. of Civil and Environmental Engineering, North Dakota State Univ., Fargo, ND 58105.

²Ph.D. Student, Dept. of Civil and Environmental Engineering, North Dakota State Univ., Fargo, ND 58105.

³Ph.D. Student, Dept. of Civil and Environmental Engineering, North Dakota State Univ., Fargo, ND 58105.

⁴Assistant Professor, Dept. of Civil and Environmental Engineering, North Dakota State Univ., Fargo, ND 58105 (corresponding author). E-mail: zhibin.lin@ndsu.edu

Note. This manuscript was submitted on November 2, 2016; approved on September 13, 2017; published online on April 9, 2018. Discussion period open until September 9, 2018; separate discussions must be submitted for individual papers. This paper is part of the *Journal of Bridge Engineering*, © ASCE, ISSN 1084-0702.

Chinchalkar 2001; Yang et al. 2004; Lee 2009; Wang and Chen 2013; Lin et al. 2014; Pavlopoulou et al. 2016) for structural condition diagnostics and damage detection. These methods are using captured sensor data to calibrate/interpret physics-based vibratory characteristics of structural systems (Salawu 1997; Chinchalkar 2001; Lee 2009; Fahim et al. 2013), including natural frequency, mode, and curvature. Although these physics-based analytical models and simulation techniques are now well established (Zou et al. 2000; Magalhães et al. 2012; Kopsaftopoulos and Fassois 2013; Masciotta et al. 2014; Comanducci et al. 2016), rapidly and accurately interpreting large amounts of data and pattern recognition still lag behind. This is a big challenge, particularly when the cable-stayed bridges are under complex operational or environmental interference in which the physics-based techniques could be incapable of recognizing and detecting abnormality.

Alternatively, another type of data analysis is the data-driven approach (Hou et al. 2000; Farrar and Worden 2013), such as the machine learning techniques that have been receiving increased attention for data mining for large-scale civil infrastructure applications (Ko and Ni 2005; Rashedi and Hegazy 2015; Gerist and Maher 2016; Jang 2016; Gui et al. 2017; Pan et al. 2018). The data-driven approaches tend to extract sensitive features from big data sets for structural diagnosis and damage detection, regardless of the complexity of physical systems. Thus, they are robust enough to provide the key information from the complex and heterogeneous sensor data, which may be no longer valid for the physics-based approaches. Some pioneer studies have been undertaken in the data-driven structural diagnosis and damage detection in structures, including using Bayesian networks (Masri et al. 2000), artificial neural networks (Zang and Imregun 2001), and support vector machines (SVMs) (Oh and Sohn 2009; Farrar and Worden 2013; Gui et al. 2017). Note that the accuracy of these data-driven methods for structural diagnosis is associated with the proper selection of feature data. From a systematic standpoint, few attempts, however, have been made to address data-driven structural diagnosis and damage detection for cable-stayed bridges in terms of the applicability of feature extraction techniques and data training. Findings from these previous studies may not fully account for the data process under various scenarios in a cable-stayed bridge. Furthermore, the data-driven approaches also expand the functionality of those physics-based conventional methods (e.g., wavelet or short-time Fourier transforms), which are defined in time-frequency series to be more robust and have adaptive tools for feature extraction (Bin et al. 2012). Also, the other time-frequency techniques, including the Hilbert-Huang transform (HHT) (Yang et al. 2004; Hsu et al. 2013) and the Teager-Huang transform (THT) (Li et al. 2010), have been proposed for the data process in aerospace and mechanical engineering (Kim and Melhem 2004). The selection of feature extraction methods is key to ensuring the effectiveness of data the process in machine learning. The signal for time-frequency feature extraction is within a short time domain. Although many time-frequency methods are available, these methods have similar limitations in the short-time domain. Thus, it could be really time-consuming and nonrealistic to run the analysis over a longer period of time. For a longer time, sampling using certain time intervals could compensate for this drawback, and the training samples in the machine learning could capture fully statistical features under those certain time intervals. Within the time interval, the time-frequency analysis could be conducted. As a result, statistic properties of longer time signals could be captured by the learning process, which could effectively avoid the averaging or subjective criteria. With this framework one could have more flexible criteria for the

selection of feature extraction methods. For instance, the wavelet transform has less sensitivity to noise, but the other methods, including the HHT and THT, have more sensitivity to damage. Thus, integration of these methods into the structural diagnosis for large-scale cable-stayed bridges could enrich the categories of feature extractions for the data-driven data process, and, in turn, open a new door for data-driven approaches with widespread implementations for large-scale civil engineering structures.

Therefore, this study aimed to develop a data-driven framework for structural diagnosis and damage detection using a SVM integrated with enhanced feature extraction techniques, striving for rapid condition assessment for large-scale cable-stayed bridges. Three representative feature extraction methods, including the wavelet transform, the HHT, and the THT, were selected. A numerical simulation was used to verify the concept and demonstrate the effectiveness and sensitivity of the data-driven damage detection for cable-stayed bridges. Moreover, a further parametric study was conducted to address the impact of damage level, damage location, sensor location, and moving loading on the data classification.

Proposed Data-Driven Techniques for Damage Detections

Advanced sensor network systems using the wireless passive networks enable the collection of massive amounts of data for SHM and damage detection (Ge et al. 2016; Pan et al. 2016). Data mining in the SHM of the cable-stayed bridges is crucial to gain key information for assessing their structural health and identifying potential damage/defects (e.g., in stay cables or decks). As stated earlier, the physics-based and data-driven methods (particularly machine learning) are two approaches for structural assessment and damage detection. A statistical pattern recognition paradigm in the SHM applications has recently been proposed (Farrar and Worden 2013; Gui et al. 2017). The data mining process is classified into four steps: (1) operational evaluation, (2) data acquisition, (3) feature extraction, and (4) statistical model development for feature classification. A framework, illustrated in Fig. 1, is proposed, displaying the data-driven workflow from a massive amount of acquired data to sensitive feature extraction. To effectively capture sensitive features of the data collected from the bridges, the framework consists of the specific seven steps, including data fusion, damage feature extraction and feature analysis, machine learning, and damage detection, as shown in Fig. 1.

Consider that actual field sensor data are very limited in the literature and may not account for the data for damage scenarios in most cases. Numerical simulation was accepted for the conceptual demonstration (Oh and Sohn 2008; Silva et al. 2016); thus, the simulated data in this paper are used. To better represent the sensor data captured in a field in which they are exposed to various operational or noise interference, different levels of noises were introduced in the data process in Step 3 (Fig. 1) in this study. Note that field data could be contaminated by various factors and be more complex than simulated data, which could cause a number of challenges in the data process. Thus, more attention will be paid to these issues in further studies.

Assuming that data type is a time series, various feature extraction methods, including the wavelet transform, the HHT, and THT, are candidates to extract damage-sensitive features from time series data. The SVM learning algorithms are specifically designed for classification between damage and undamaged cases, in which the radial basis function (RBF) kernel in this

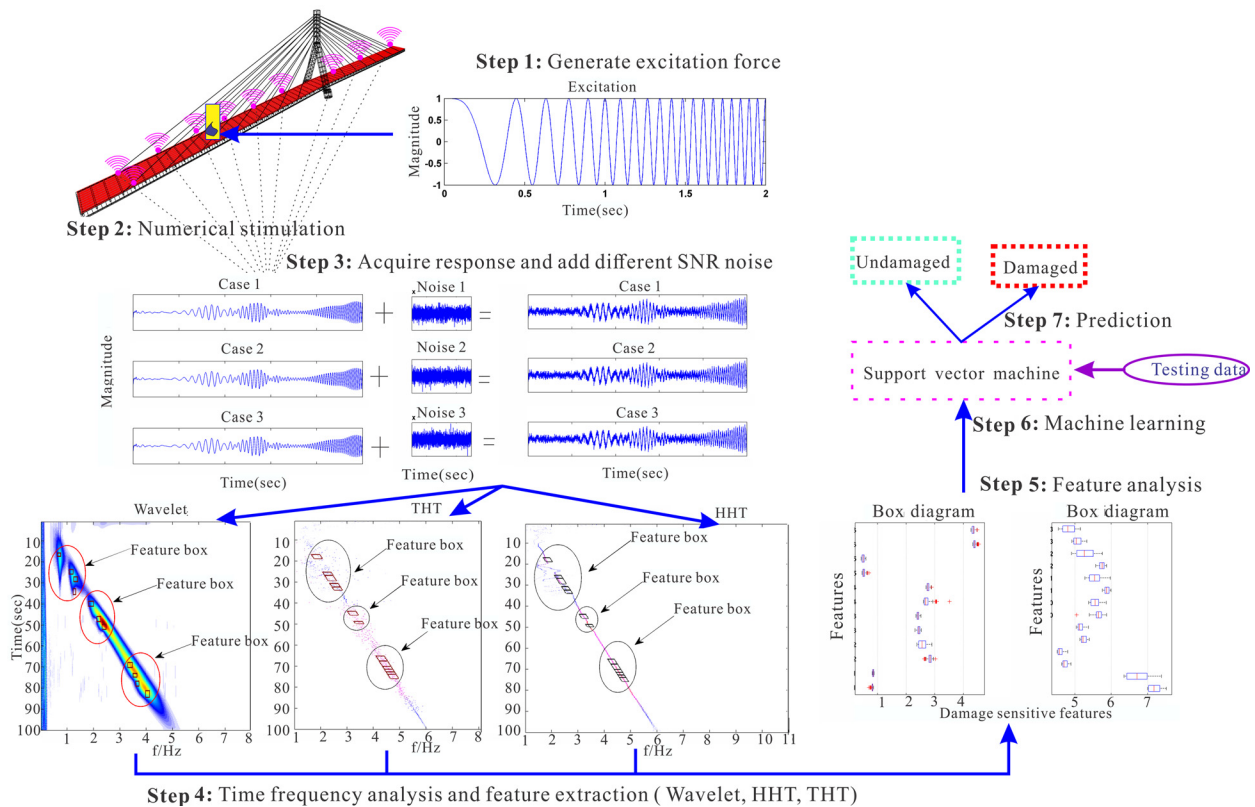


Fig. 1. Framework of data-driven data mining process for SHM and damage detection (Note: SNR = signal-to-noise ratio)

paper is chosen as the kernel function, as detailed in the following sections.

Data-Driven Feature Extraction and Data Processing Techniques

Dynamic characteristics of cable-stayed bridges exhibit apparent nonstationary and nonlinear behavior (Bornn et al. 2010). Time-frequency analysis is effective for tracking the change of a system and its nonlinear behavior (Li et al. 2010), and the conventional techniques are mostly encompassed by the wavelet transform, short-time Fourier transform, and Wigner-Ville distribution (Feng et al. 2013). These methods have some drawbacks in data analysis, such as high computational time and less adaptive features. The emerging techniques, including the HHT and THT, have demonstrated great potential for data-driven time-frequency analysis (Li et al. 2010; Yang et al. 2004; Hsu et al. 2013). The HHT and THT display a sparse feature and have no limitation by the Heisenberg uncertainty principle compared with their conventional counterparts, although these methods have their own limitation in noise sensitivity. The literature review shows that few attempts have been made to address the impact of various feature extraction methods on structural condition assessment and damage detection, particularly for large-scale cable-stayed bridges. Thus, the authors selected three representative feature extraction methods and the data process using supervised machine learning, including the wavelet transform, the HHT, and the THT, which is discussed in the next section.

Wavelet Transform

Wavelet transform, due to the excellent local zooming property of the wavelet, is an effective tool for time-frequency decomposition

for analyzing nonstationary signals (Daubechies 1990; Sun and Chang 2002; Yan et al. 2014), including the discrete wavelet transform (Daubechies 1990), the wavelet packets transform (Sun and Chang 2002), and the continuous wavelet transform (Yan et al. 2014). Among them, the continuous wavelet transform could provide more smooth and specific time-frequency resolution throughout the signals over the other two methods. Thus, the multiresolution continuous wavelet analysis is used in this paper to decompose the signal in time and frequency domain with a Morlet mother wavelet (Yan et al. 2014). The continuous wavelet transform of a continuous signal, $x(t)$, is defined as (Yan et al. 2014)

$$Wx(a, b) = x \otimes \psi_b, \quad a(t) = \frac{1}{\sqrt{a}} \int_{-\infty}^{+\infty} x(t) \psi^* \left(\frac{t-b}{a} \right) dt \quad (1)$$

where ψ and ψ^* = basic function and its complex conjugate; and a and b are the scale and translation factors, respectively. A signal through Eq. (1) is to be projected into a two-dimensional (2D) time-scale plane and can be achieved by a pair of Fourier transform and inverse Fourier transforms [Eq. (2)]. The form in the frequency domain is expressed as (Yan et al. 2014)

$$Wx(a, f) = \frac{1}{\sqrt{a} 2\pi} \int_{-\infty}^{+\infty} \left[\left(\frac{t-b}{a} \right) dt \right] e^{-j2\pi f \tau} db = \mathcal{F}\{Wx(a, b)\} \quad (2)$$

where $\mathcal{F}\{\cdot\}$ denotes the Fourier transform. By using the inverse Fourier transform, Eq. (2) is converted into the time domain as

$$Wx(a, t) = \mathcal{F}^{-1}\{Wx(a, f)\} \quad (3)$$

where $\mathcal{F}^{-1}\{\cdot\}$ denotes the inverse Fourier transform. The variation of the scale factor, a , could yield different resolutions in different domains. A relatively small-scale factor could provide a high resolution in the time domain, whereas one could have better resolution in the frequency domain with an increase of the scale factor. As a result, the continuous wavelet transform is capable of generating better adjustable time and frequency resolutions at any scale than the other two methods. Note that the continuous wavelet transform is abbreviated as the wavelet transform for simplicity, unless otherwise noted.

HHT

The HHT is a novel technique of signal decomposition with many interesting properties. The HHT consists of empirical mode decomposition (EMD) and Hilbert spectral analysis through the generation of intrinsic mode function (IMF) using the EMD (Mandic et al. 2013) and the HHT time-frequency description of a time series for the obtained IMFs. The process of EMD to decompose the simple embedded oscillatory mode from any signal $x(t)$ has been documented in detail (Huang et al. 1971).

The EMD acts essentially as a dyadic filter bank resembling those involved in wavelet decompositions (Flandrin et al. 2004). The frequency bands range from high to low as the IMFs increase. The residue r_n represents the central tendency of signal $x(t)$ (Yu et al. 2005). By using this algorithm, the beginning $h_{1k}(t)$ will contain the highest frequency. The Hilbert transform is used to describe the IMFs

$$H[h_{ik}(t)] = \frac{1}{\pi} \int_{-\infty}^{+\infty} \frac{h_{ik}(\tau)}{t - \tau} d\tau \quad (4)$$

After using the Hilbert transform for each IMF, the signal $x(t)$ can be defined as follows:

$$x(t) = \operatorname{Re} \sum_{i=1}^n a_i(t) e^{j \int \omega_i(t) dt} \quad (5)$$

where Re stands for “real part”; $\omega_j(t) = 2\pi f_j(t)$; and $j = \sqrt{-1}$. The Hilbert-Huang time-frequency spectrum $H(\omega, t)$ can be expressed as follows:

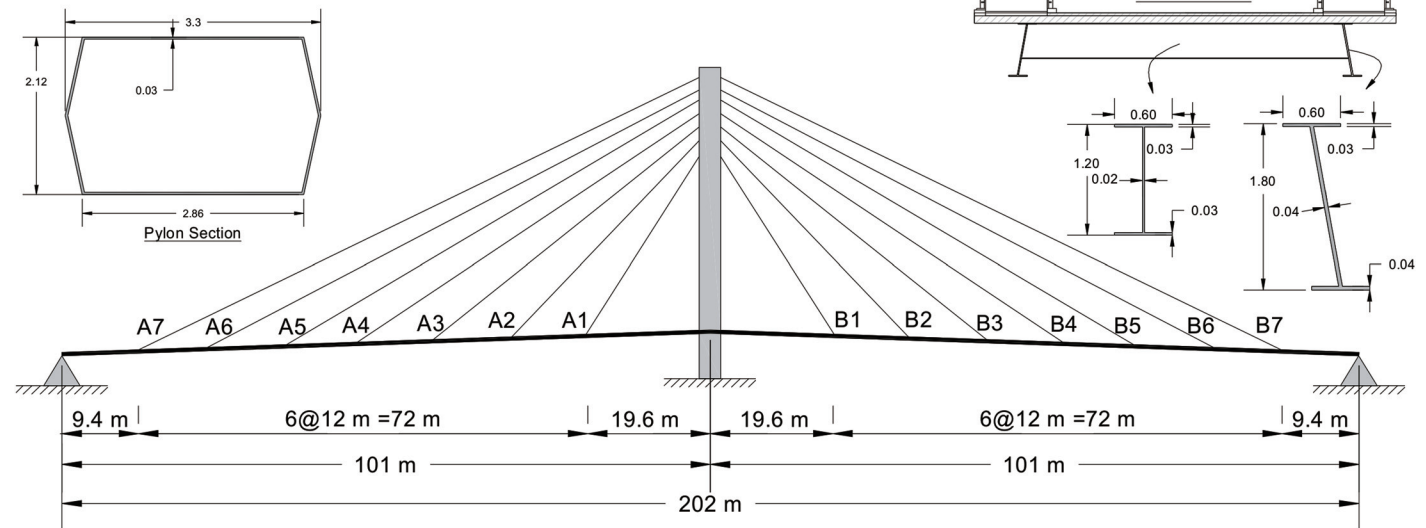


Fig. 2. Manavgat cable-stayed bridge layout and the cross section of the structural members

$$H(\omega, t) = \operatorname{Re} \sum_{i=1}^n a_i(t) e^{j \int \omega_i(t) dt} \quad (6)$$

THT

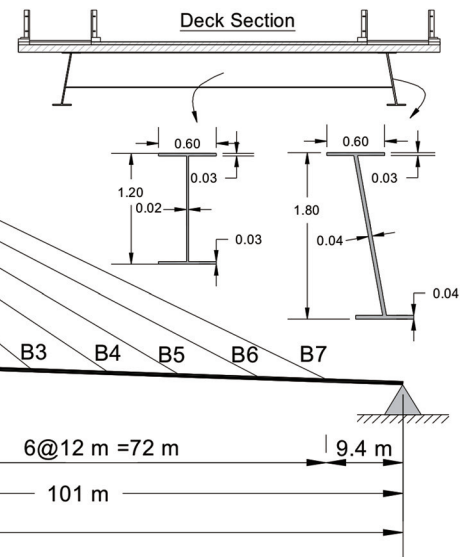
The THT was introduced by Cexus and Boudraa in 2006 (Cexus and Boudraa 2006). It has been used in the fields of aerospace and mechanical engineering (Cexus et al. 2010; Junsheng et al. 2007; Li et al. 2009). This method combines the EMD and Teager energy operator (Flandrin et al. 2004). The IMFs are demodulated into instantaneous frequency (IF) and instantaneous amplitude (IA) signals. The Teager-Kaiser energy operator (TKEO) is selected as an energy demodulation method to simultaneously track these IF and IA components (Bouchikhi et al. 2014). The TKEO has high time resolution and ease of operation, while maintaining the meaningful quantity frequency and amplitude of each IMF. The signal $x(t)$ can be expressed as the following form using the THT:

$$x(t) = \operatorname{Re} \sum_{i=1}^n a_i(t) e^{j \int \omega_i(t) dt} + r_n(t) \quad (7)$$

This equation can be written as a three-dimensional (3D) figure $(t, f_i(t), a_i(t))$. The Teager-Kaiser spectrum (TKS) can be defined as follows:

$$\operatorname{TK}(t, f) = \begin{cases} a_1(t) f_1(t) \text{ and } t \text{ for IMF1} \\ a_2(t) f_2(t) \text{ and } t \text{ for IMF2} \\ \vdots \\ a_n(t) f_n(t) \text{ and } t \text{ for IMF}n \end{cases} \quad (8)$$

Eq. (8) shows that the time-frequency distribution has K one-dimensional (1D) trajectories to be nonzero. Thus, the number of points is KT dimensions, which are concentrated in some trajectories and are smaller than other time-frequency spectrums, such as the wavelet transform.



Machine Learning Using SVM

The SVM is one of the effective supervised machine learning techniques in data classification (Farrar and Worden 2013; Gui et al. 2017; Pan et al. 2018). In this method, a hyperplane is used to separate the two different classes of samples based on the SVM training algorithm (training data) and by maximizing the “margin,” which is the distance from the hyperplane to the closest data points in either class. By defining the kernel function as the inner product, the data can be mapped into a higher dimensional feature space; thus, the SVM can be applied to nonlinear classification problems. For this purpose, various kernel functions can be used, such as the linear, polynomial, or Gaussian RBF.

Because the acquired data are not always separable, it is reasonable to ignore the outlier data points and use the soft margin SVM, which includes the slack variable ξ_i and the error penalty c . Thus, the margin is defined as (Farrar and Worden 2013)

$$\text{Margin} = \frac{2}{w^2} \quad (9)$$

Table 1. Test Cases Used in the Data Analysis

Label	Condition	Description
Undamaged states (1–4)		
1	Undamaged	Baseline condition
2	Undamaged	Added 8% additional mass uniformly on the bridge deck (static)
3	Undamaged	AASHTO HL-93 design truck moving through the span (dynamic, $v = 10$ m/s)
4	Undamaged	AASHTO HL-93 design truck moving through the span (dynamic, $v = 20$ m/s)
Damaged states (5–15)		
5	Damaged	10% reduction of cable area at the A4 (one side)
6	Damaged	20% reduction of cable area at the A4 (one side)
7	Damaged	30% reduction of cable area at the A4 (one side)
8	Damaged	40% reduction of cable area at the A4 (one side)
9	Damaged	50% reduction of cable area at the A4 (one side)
10	Damaged	20% reduction of cable area at the A2 (one side)
11	Damaged	20% reduction of cable area at the A6 (one side)
12	Damaged	40% reduction of cable area at the A2 (one side)
13	Damaged	40% reduction of cable area at the A6 (one side)
14	Damaged	40% reduction of cable area at the A4 (one side) + moving load (10 m/s)
15	Damaged	40% reduction of cable area at the A4 (one side) + moving load (20 m/s)

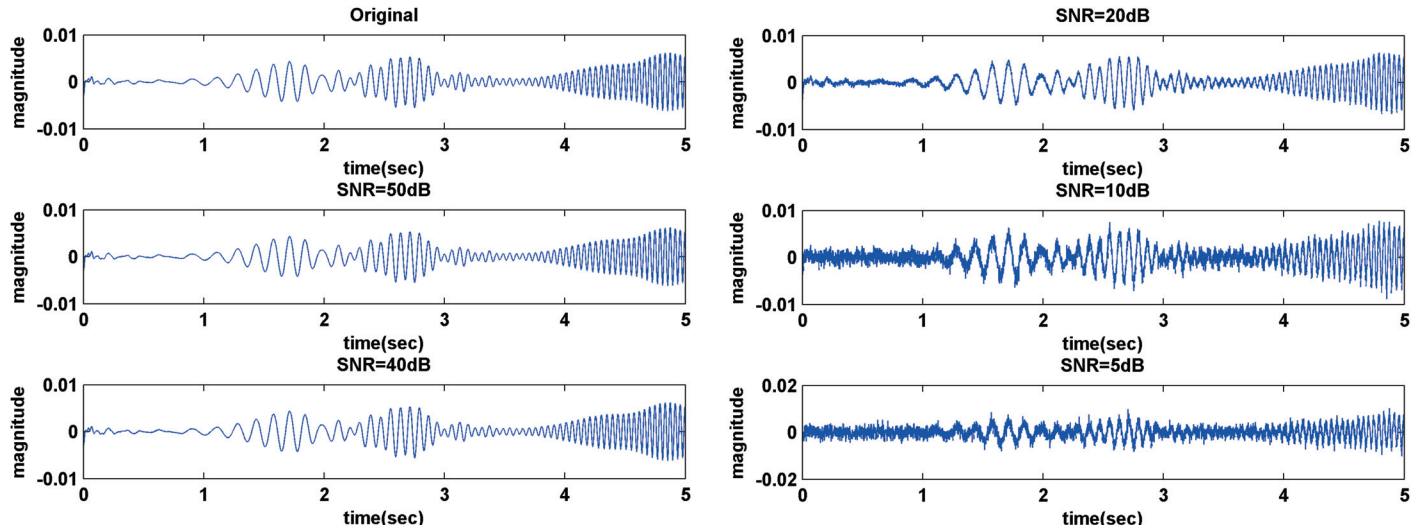


Fig. 3. Framework of data-driven data mining process for SHM and damage detection

Therefore, the optimization problem is defined in Eqs. (10a) and (10b)

$$\min\left(\frac{1}{2}\|\mathbf{w}\|^2 + c \sum_{i=1}^N \xi_i\right) \quad (10a)$$

$$\text{Subject to } y_i(\mathbf{w}, \mathbf{x}_i + b) \geq 1 - \xi_i, \quad \xi_i \geq 0 \quad (10b)$$

where w and b = vector and scalar that define the position of the hyperplane, and ξ_i = measure of how much an observation fails to satisfy the target margin. Therefore, the nonlinear decision function can be defined using the Lagrange multipliers algorithm and by solving the dual optimization problem as (Farrar and Worden 2013; Gui et al. 2017)

$$f(x) = \text{sign} \left[\sum_{i=1}^N \alpha_i y_i K(x, x_i) + b \right] \quad (11)$$

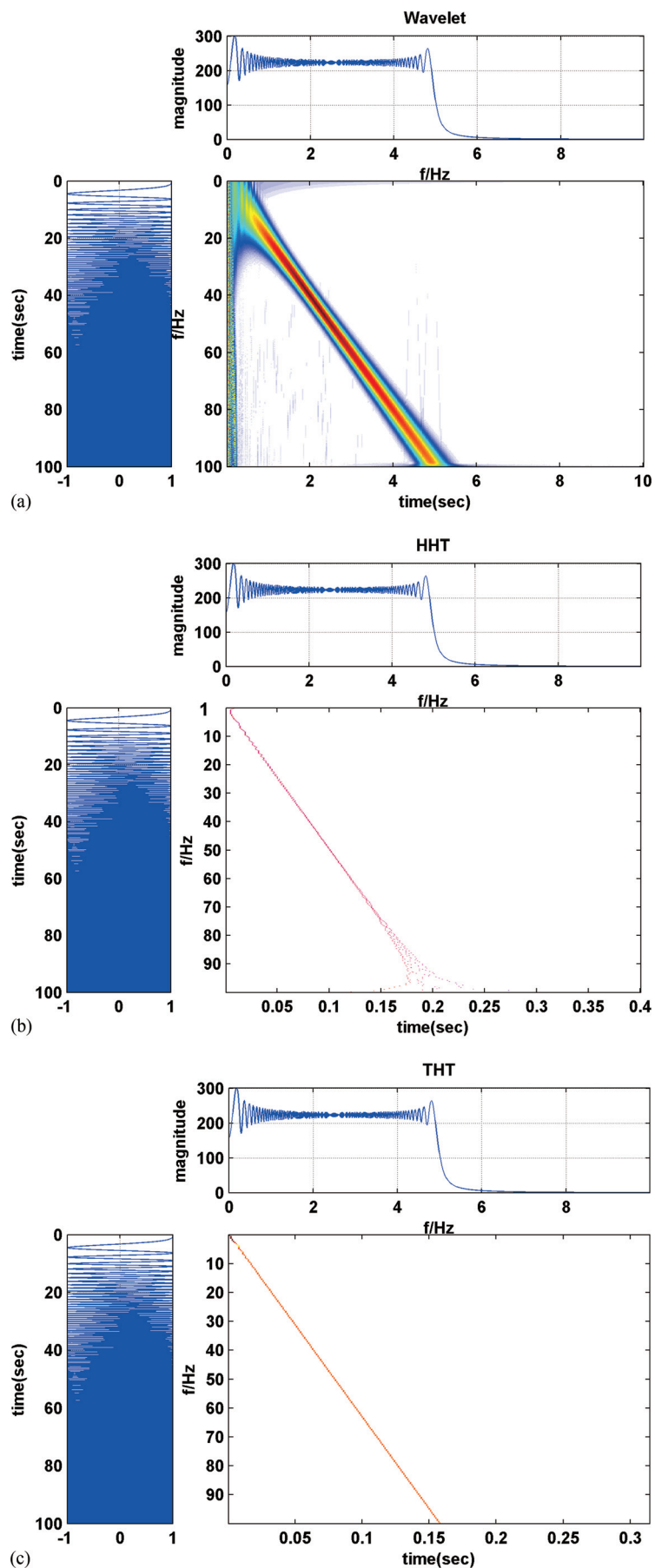


Fig. 4. (a–c) Input sweeping excitation forces under three different methods

Case Study

Prototype Structure

The Manavgat cable-stayed bridge, located in Turkey, was selected from the literature (Atmaca et al. 2015; Atmaca et al. 2014) for numerical analysis. The layout and the cross sections of the structural members of the bridge are shown in Fig. 2. The bridge is 202 m long with equal spans of 101 m, and a total of 28 steel cables connect the 13.7-m wide deck to the λ -shape steel tower. The tower is approximately 42 m high with a hollow hexagonal cross section and placed on a concrete footing. The deck has a composite cross section, which consists of 25 cm of concrete, 10 cm of pavement, and two continuous steel girders that are laterally restrained by I-beams that are each approximately 3 m.

The distance of the nearest cable to the center of the pylon is 19.6 m, and the distance between the cables is 12 m. The last cables are connected to the deck 9.4 m away from the abutments. Cables A1–A7 include 14, 16, 19, 19, 22, 19, and 24 strands, respectively. Each strand has a cross-section area of 150 mm^2 , an elastic modulus of 197 GPa, and the ultimate strength of 1,860 MPa. The elastic

moduli for the concrete and steel materials have been defined as 34 and 200 GPa, respectively.

Numerical Simulation

Nonlinear time history analyses were performed using commercially available SAP2000 software. The following assumptions were made to idealize the finite-element modeling: (1) the deck is continuous, (2) the cables carry only axial forces, and (3) the soil-structure interaction and the effects of nonstructural components are negligible. To calibrate the model, the modal analyses revealed that the first six periods of the bridge predicted by this study, ranging from 0.309–0.825 s, matched well with those in the literature (Atmaca et al. 2015; Atmaca et al. 2014).

Because the damping ratio is considerably high and the natural frequencies of the bridge are very close to each other, instead of impact load, a chirp excitation with time-dependent amplitude and frequency (sweeping frequency) was applied to the deck at the midpoint of the left span. The acceleration of all 28 joints (end of cables) was captured (using accelerometer sensors). The excitation had a sweeping signal from 0–5 Hz. The sampling rate of this model was 100 Hz.

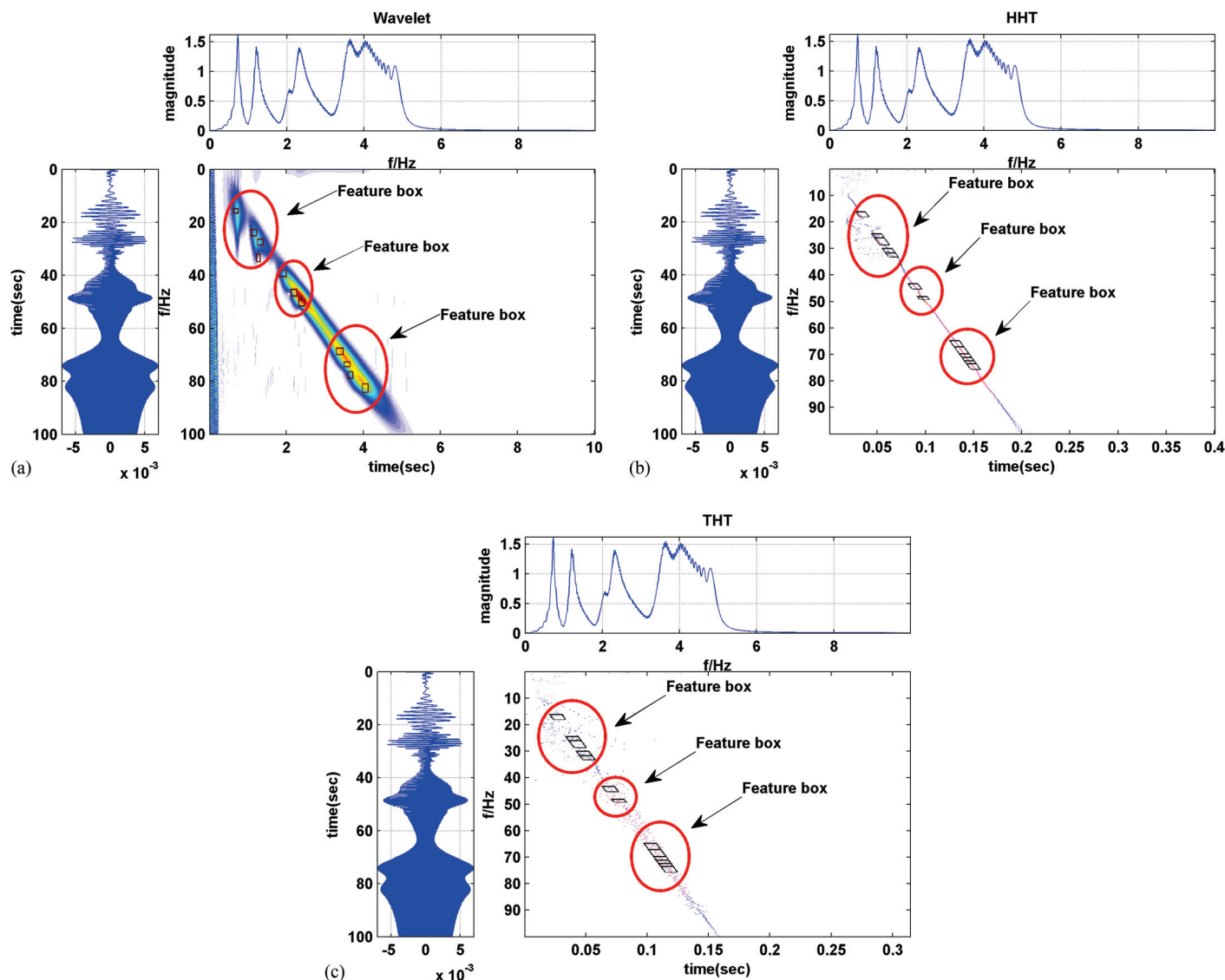


Fig. 5. (a–c) Feature extraction from time-frequency distribution planes

A total of 15 test cases were defined to verify the effectiveness and accuracy of the proposed approaches, as listed in Table 1. The dynamic responses at the location of A4 in Fig. 2 were selected to demonstrate the concept, unless stated elsewhere. State 1 was used as the baseline condition without any damage, whereas States 2–4 were designed to simulate the bridge fully loaded with vehicles at both static load and with an AASHTO HL-93 (AASHTO 2008) moving design truck for the consideration of the operational influence. States 5–15 were designed for various damage scenarios. Among them, States 3–9 were designed to simulate the defects reducing cable stiffness, under five different damage levels in stay cables (from 10 to 50% of cable area at location A4). States 10–13 were used to determine the effects of damage locations on data classification, in which State 11 represents the location of a quarter span

and State 10 is located at the three-quarter span. The last two cases were designed to account for the combined effects of moving loading as well as the reduction of cable area, in which two speeds of the design truck are 10 and 20 m/s, respectively, in accordance with the operational conditions at States 3 and 4.

Introduction of Noise Interference in Data

Noise is a challenge for damage detection (Simonovski and Bolte 2003; Pakrashi et al. 2007); therefore, in this study, noise was added to the response of the bridge signals. A different noise level was selected as the representative sensor data for SVM learning to check the sensitivity of the damage feature. The training data for SVM were simulated by adding different noises based on the signal-to-

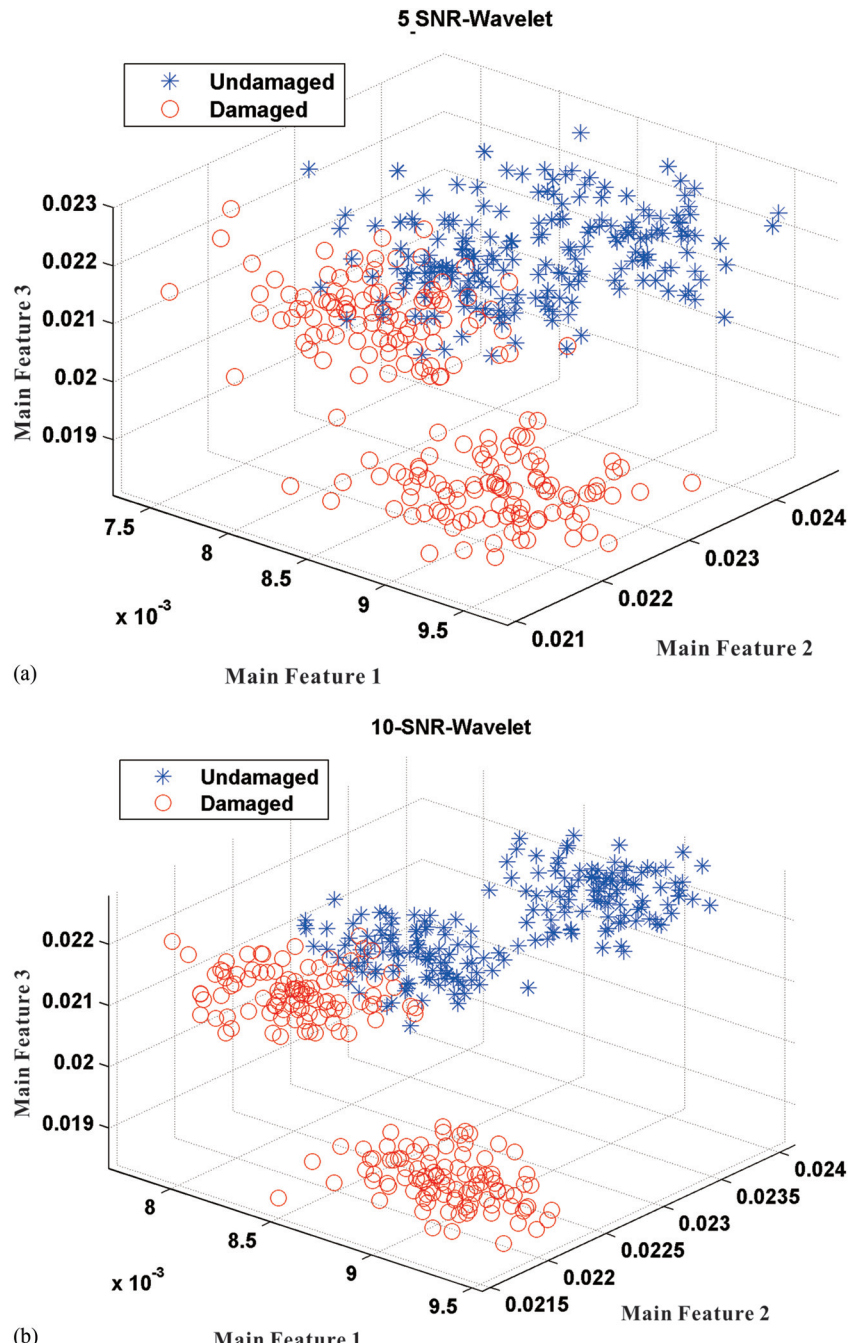


Fig. 6. (a–i) Scatter plots of three main features

noise ratio (SNR), which represents the ratio of the signal strength to the background noise strength (Simonovski and Bolte 2003; Pakrashi et al. 2007). The SNR is usually described in the decibel (dB) scale as

$$\text{SNR}_{\text{dB}} = 10 \log_{10} \left(\frac{P_{\text{signal}}}{P_{\text{noise}}} \right) \quad (12)$$

where P_{signal} and P_{noise} = average power of signal and noise, respectively. Five different levels of SNRs are used in this study: 5, 10, 20, 40, and 50 dB (Fig. 3). In addition, for each SNR level, 100 samples were selected to train the SVM model ($4 \text{ cases} \times 5 \text{ SNRs} \times 100 \text{ samples} = 2,000 \text{ signals in total}$). The final samples were separated randomly into two equal parts as training data and testing data. To prevent overfitting of the problem, the cross-validation procedure was used to get the effective estimation of the models. The testing

data were used to evaluate the performance of the machine learning algorithm. For simplicity, each group of samples was named in accordance with the feature extraction method and the level of the SNR. For example, 20-SNR-wavelet denotes the data predicted by the wavelet with a SNR of 20 dB, whereas 50-SNR-THT represents the data predicted by the THT method with a SNR of 50 dB.

Results and Discussions

Feature Extraction and Sensitivity

The sampling frequency of this model is 100 Hz. A sweeping signal from 0 to 5 Hz was excited at the midpoint of the left span. The time-frequency representations of the wavelet transform, HHT, and THT under the sweeping signal are plotted in Figs. 4(a–c). Clearly,

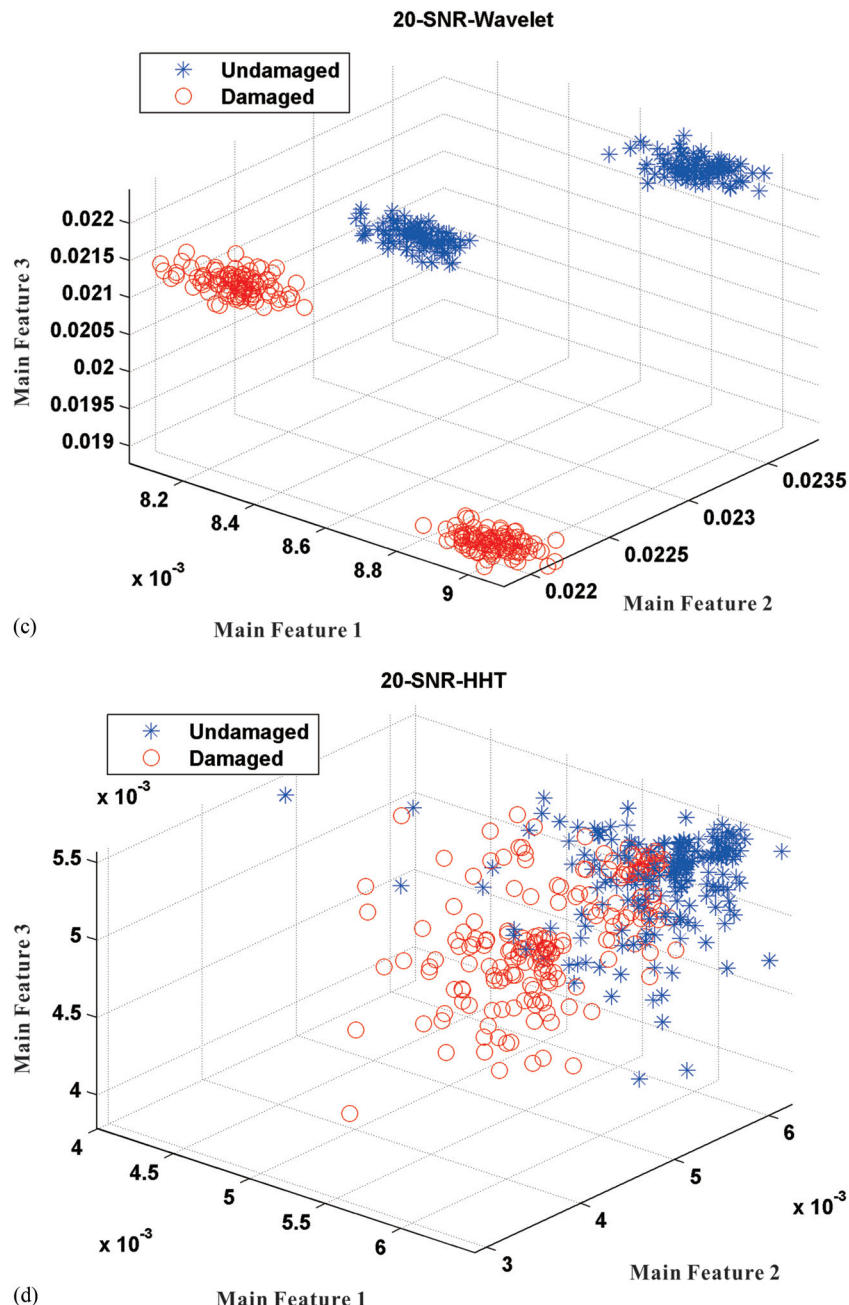


Fig. 6. (Continued.)

for a regular signal, the THT, due to the high time resolution, had the highest concentration and the fewest boundary effects compared with the other two methods. Although the HHT has sparse characteristics similar to that of THT, the HHT still displayed certain boundary effects under regular signals, as shown in Fig. 4(b). The wavelet had the highest boundary effects with an apparently wide band. Further comparison of the time-frequency distribution predicted by the HHT and THT demonstrated that the THT is more sensitive to the change of signal.

The time-frequency plane is capable of providing more key information than that of the time domain or frequency domain field. It is also more effective for tracking a number of sensitive features from this plane. The 2D box is used to separate the damage-sensitive features, as shown in Fig. 5.

A feature selection process, the time-frequency box, was used to choose the best sensitive feature (Lin and Qu 2000). The concept of a feature selection process is based on counting the maximum number of outline samples that exceed the 5 and 95% of the feature value at the baseline condition. The feature is also relevant to the main frequency and main time domain point, as reported in the literature (Lin and Qu 2000). The mean value of each box contained a time-frequency representation point, which is used to eliminate the influence of noise in the signal as

$$\text{Feature}_i = \frac{\sum_{i=1}^N \text{TFR}_i}{N} \quad (13)$$

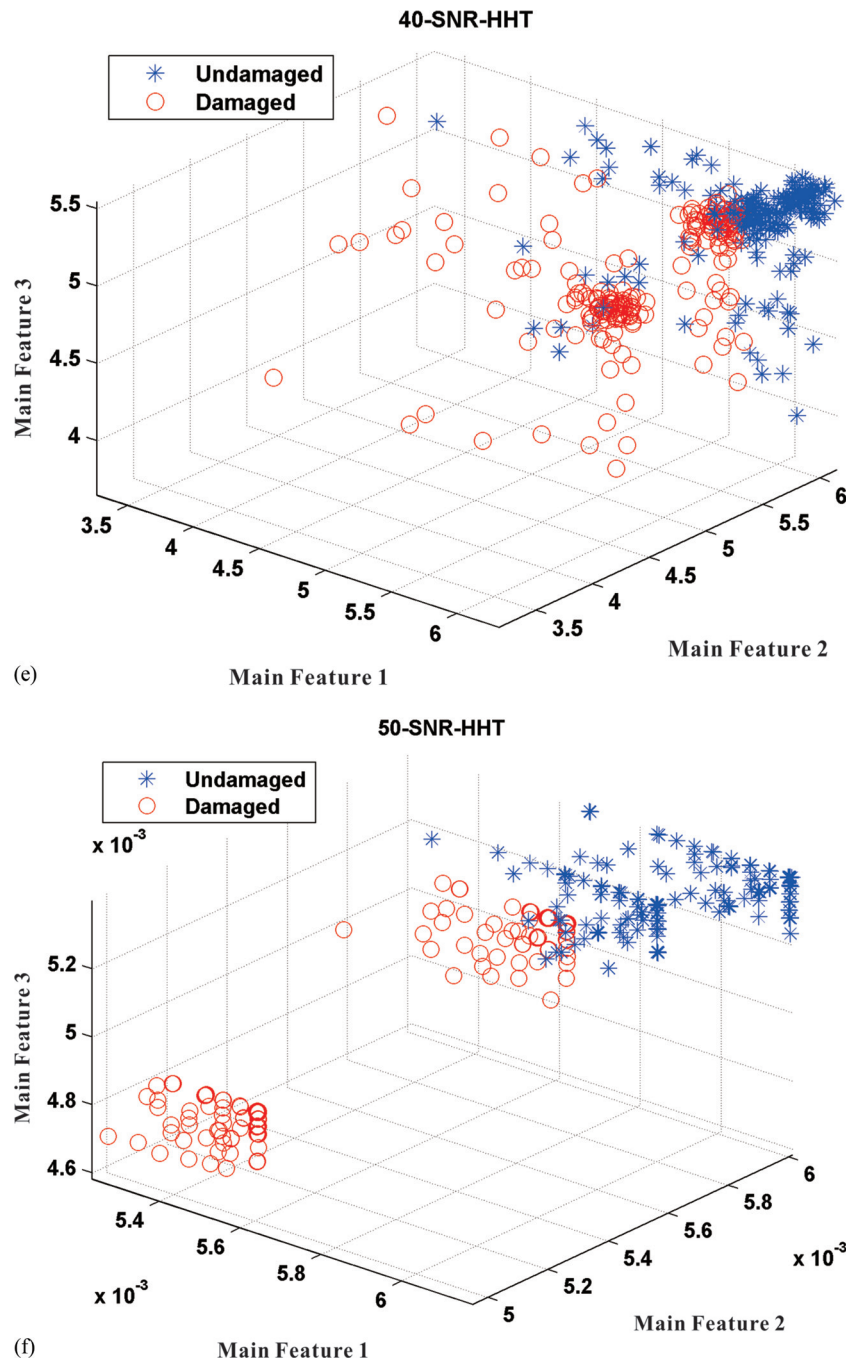


Fig. 6. (Continued.)

where N = number of time-frequency representation point; and TFR_i = time representation point in Figs. 5(a–c). The wavelet function is used in the wavelet transform. Different boxes throughout the entire time-frequency domain are used to select the damage features, as shown in Fig. 5(a). The box information represents all the dynamic information of the response of the signal; thus, there are 11 boxes covering the entire main frequency field. For the HHT and THT features in Figs. 5(b and c), the selected box is somewhat different from the wavelet, and a total of 13 parallelogram boxes have been selected. The average of the time-frequency representation point, which is greater than zero in the box, has been chosen as the damage feature

$$\text{Feature}_i = \frac{\sum_{i=1}^N (\text{TFR}_i > 0)}{N} \quad (14)$$

Effectiveness of Various Feature Extraction Methods and Data Training

To demonstrate the cost-effectiveness of each feature extraction in computation, the consumed time was determined under the identical situation using *MATLAB* software. Clearly, the wavelet has a computation time of 6.996 s, which is longer than those of the HHT or THT by 0.775 s or 0.7201 s, respectively. As discussed previously,

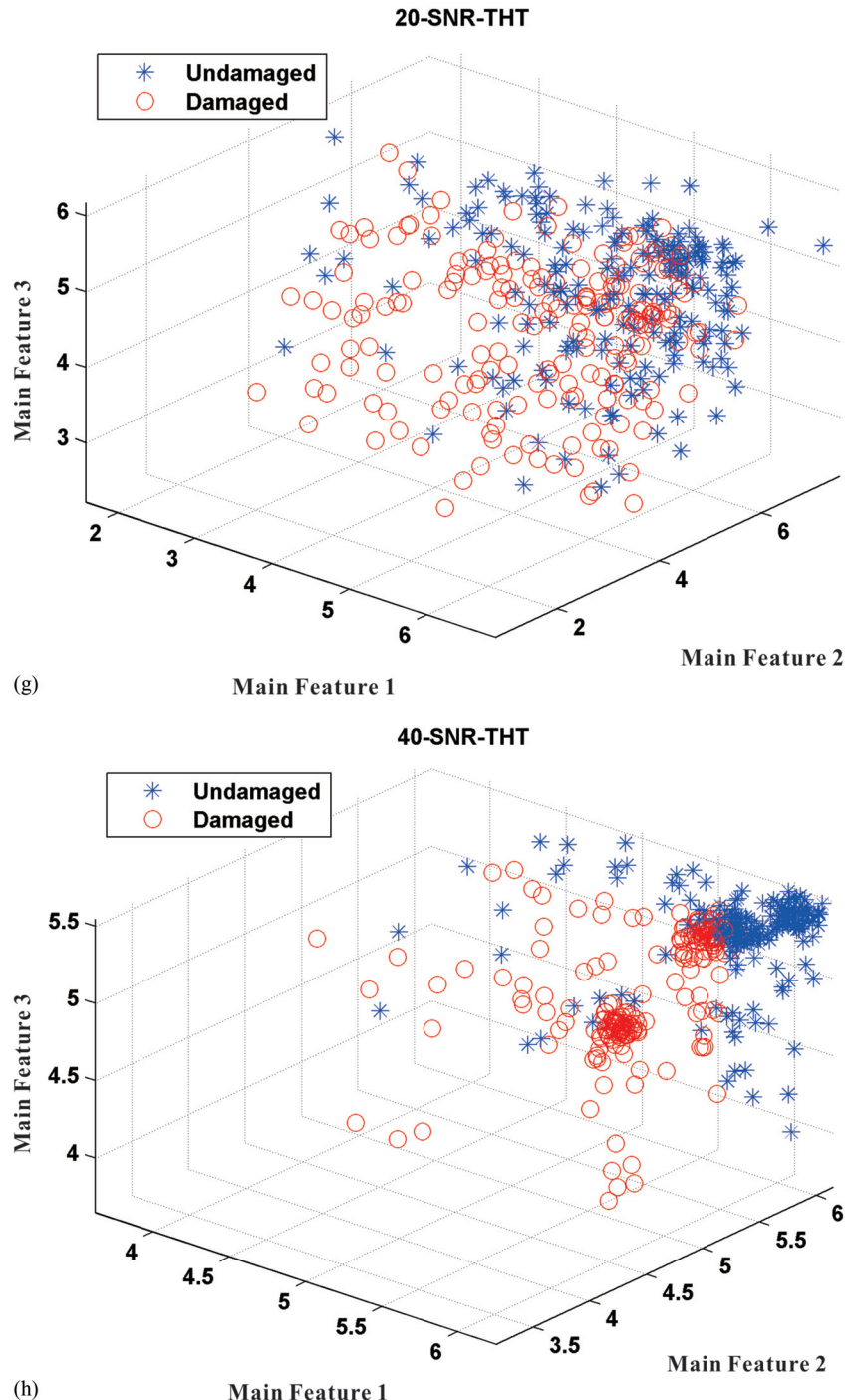


Fig. 6. (Continued.)

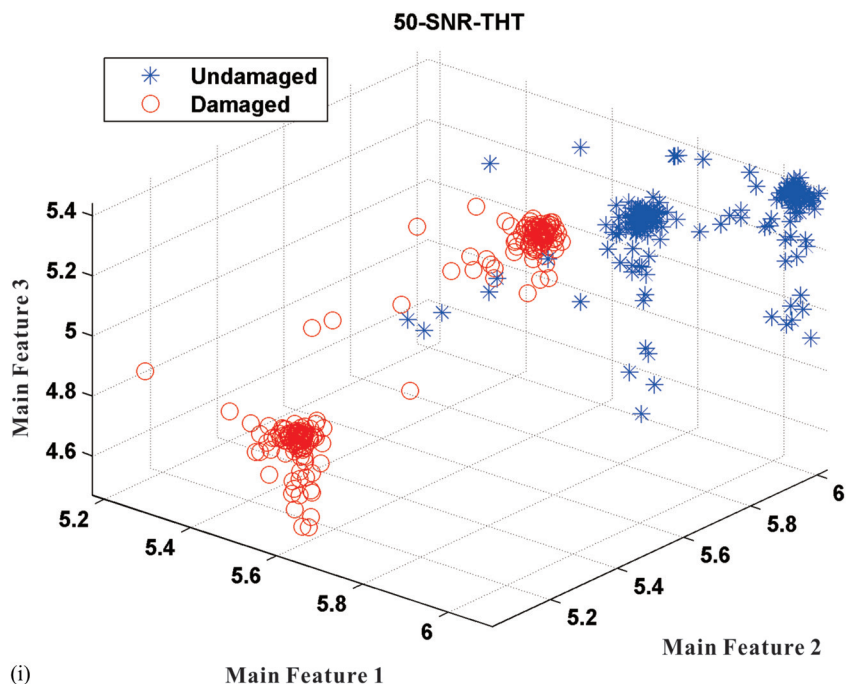


Fig. 6. (Continued.)

the HHT and THT algorithms have great potential for data-driven time-frequency analysis, particularly in terms of a sparse feature and no limitation by the Heisenberg uncertainty principle; thus, they perform approximately 10 times faster than the wavelet algorithm. Note that such a comparison is only for the demonstration of time consumption under current identical computation capacities, and other resources could compensate for their computation capacities.

To better understand the performance of the machine learning techniques, the selection of effective and sensitive damage features are in high demand. A perfect damage-sensitive feature is theoretically sensitive and robust to all kinds of damage, even under high variations and other interference. The data identification was demonstrated using the 3D scatter plot shown in Fig. 6, in which the circles and stars denote individual specimens under damage and undamaged states, respectively. Note that the main feature of each feature extraction method should be constant when estimated based on the data obtained from the numerical model. However, the influence of the different ratios of noise and the presence of operational conditions as well as damage could make the data separate. As clearly illustrated in Figs. 6(a–i), all nine plots exhibit a significant difference in data trend to allow clear identification of undamaged or damaged cases. The feature is expected to have a different cluster accordingly, for example, for the case of the 20-SNR-wavelet shown in Fig. 6, there exist four clusters and each cluster is totally separated. Clearly, three different feature extraction methods could help to maintain a high sensitivity to the presence of damage, when the SNR is under a certain level. The cluster appeared for the wavelet method as the SNR increased from 5 to 20 dB. In contrast, the clusters of the HHT and THT started as the SNR varied from 20 to 50 dB. That is, the wavelet has a lower divergent than HHT and THT, when the SNR is equal to 20 dB.

The feature vectors were split in the test and training matrices. The training matrix was composed of different features from 50 of 100 simulated signals that have different noise levels of SNR. Thus, for each SNR scenario, the training matrix with a dimension of [Feature number] \times [Cases \times 50] was used for the SVM to learn the underlying distribution and dependency of all the damage and

undamaged states. During the testing process, the SVM was expected to detect the defects (reduction of cable stiffness in this paper) from the original conditions when the features are used in Cases 5–13, even in the presence of operation effects.

To further verify the accuracy of the data-driven SVM method in this paper, the receiver operating characteristic (ROC) curve and area under the curve (AUC) were used (Gui et al. 2017). Both methods also help to determine how accurate the proposed damage identification is for distinguishing between undamaged and damaged cases. The ROC curves of testing groups were plotted for all 11 cases, as shown in Figs. 7(a–c). Qualitatively, the wavelet feature-based curves go through the left upper corner, suggesting that it has the best accuracy in damage classification, when the SNR is larger than 20 dB, as shown in Fig. 7(a). The ROC curves demonstrated that the wavelet has better accuracy when distinguishing the damage cases from undamaged data than those of the HHT and THT, when the noise of signal is assigned as 20 dB. Fig. 7(c) shows that all the damage features have greater accuracy, when the SNR reaches up to 40 dB or greater. The plots also demonstrate that the wavelet feature extraction has less impact by noise. Moreover, the wavelet performs better than that of THT with a SNR of 40 dB, even when the SNR in the wavelet method is equal to 10 dB.

Using the levels of the AUC as acceptance criteria has been widely accepted in clinical studies (Fan et al. 2006). The AUC values for each case are listed in Table 2, in which the value of the $AUC = 1$ denotes a 100% precise prediction, and the predicted results will be unacceptable when the ROC curve has an $AUC \leq 0.75$. As clearly illustrated in Fig. 7(c), the data predicted by the THT with a SNR of 20 dB will not be acceptable because it has a low value of $AUC = 0.7344$, which is smaller than the threshold of 0.75 (Table 2).

Damage Detection and the Effects of Major Factors on Its Effectiveness

From an engineering standpoint, engineers may be concerned about the effectiveness of damage identification, what levels the damage/

defects are at, and the sensitivity of the techniques that the sensor should be placed. Therefore, a further parametric study was conducted in this paper and the following discussions are characterized by major factors of interest, including effects of damage level, damage location, sensor location, and moving load.

Effects of Damage Level on Data Classification

As initially designed in Table 1, the introduction of stiffness degradation in stay cables by reducing the cross-sectional area of a cable by 10–50% was done to simulate various damage levels. The

damage index (DI) is defined as the values from the feature vectors as follows:

$$DI_i = \sum_{i=1}^N \alpha_i \times \text{Label}_i \times \text{Kernel}(\text{Fea}_i, \text{Feature}_i) + b \quad (15)$$

where Label_i , α_i , b , and Feature_i are derived and selected as the support vector points from the training process, respectively; and Fea_i is the feature from the input data, while Feature_i is the resulting feature, as predicted by Eq. (14). This index helps to assess the

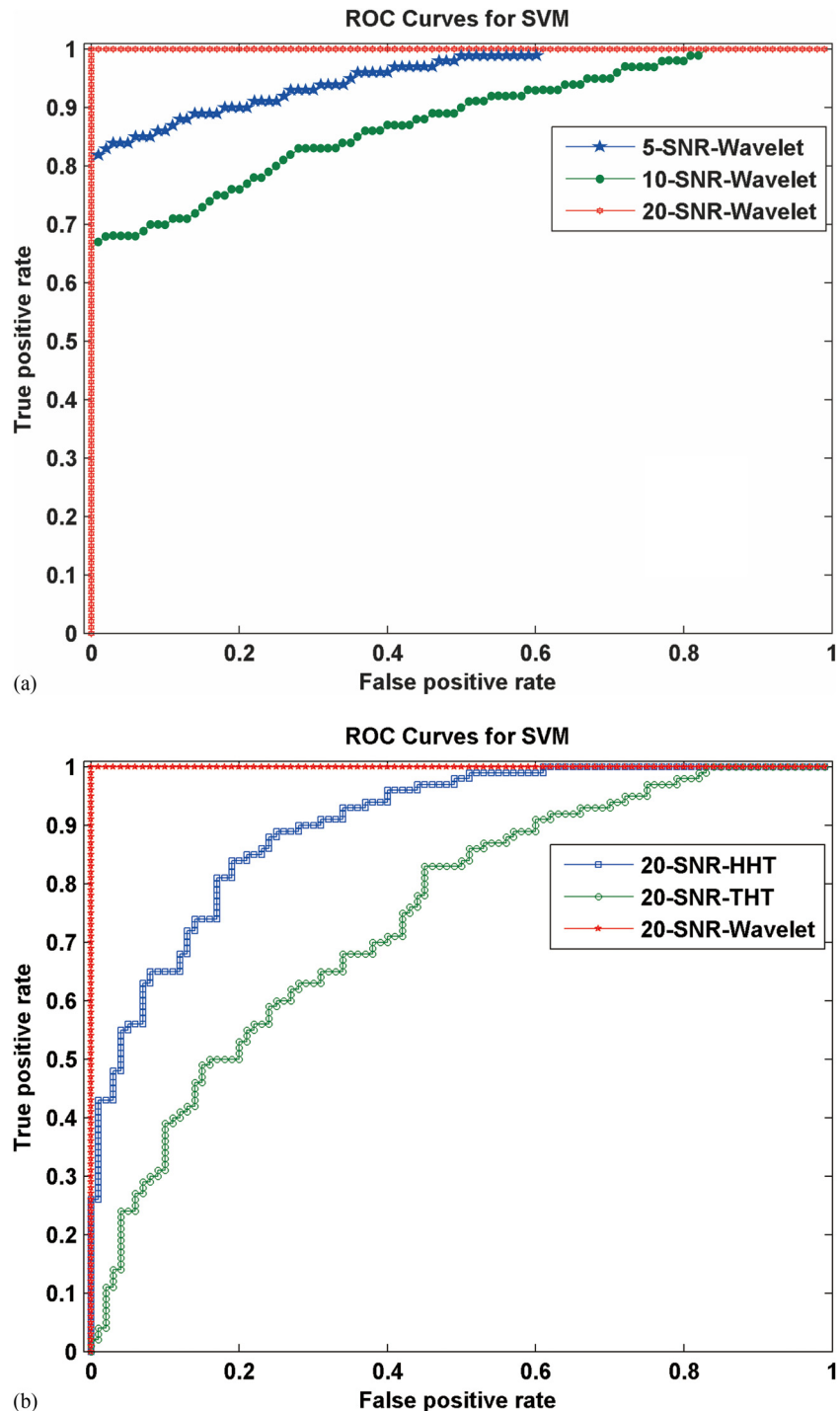


Fig. 7. (a–c) ROC curves for accuracy of the data training using three feature extraction methods

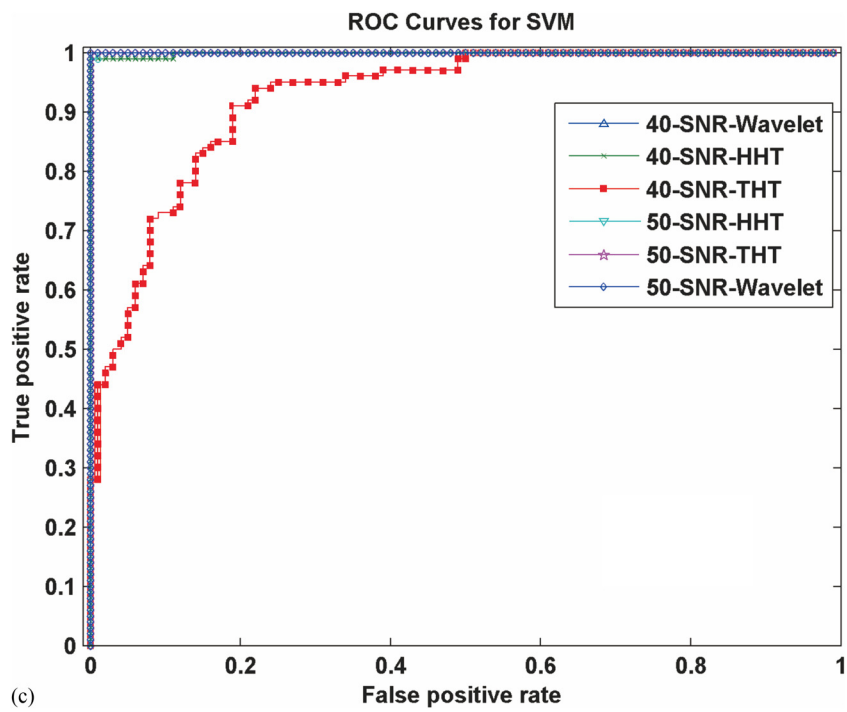


Fig. 7. (Continued.)

Table 2. AUC Values of Different Methods and Various Levels of the SNR

SNR/dB	Algorithm		
	Wavelet	HHT	THT
5	0.9688	—	—
10	0.9792	—	—
20	0.9900	0.8912	0.7344
40	1.0000	0.9889	0.9134
50	1.0000	0.9899	0.99

performance of the classifiers of the SVM with enhanced feature extraction methods. Figs. 8(a–f) plot the DIs of different damage scenarios along with a threshold based on the 95% cutoff of the baseline condition.

As shown in Figs. 8(a–f), a threshold at 95% of the undamaged state shown by the dashed line is used to discriminate the damage and undamaged states. Each slot represents a state, as labeled in Figs. 8(a–f) and defined in Table 1, whereas damage states are plotted in the first column and undamaged ones in other columns. Clearly, the entire scenario shows a great classification performance, regardless of the different feature extraction methods. Specifically, the results in the THT and HHT methods exhibit clear discrimination between each damaged state and apparently have a separable relationship between the damaged and undamaged states, even under operational and environmental variability. As discussed earlier, the data classification could be a challenge with an increase in noise level. As illustrated in Fig. 8(b), data points show much higher scatter due to the higher level of noise. Because the machine learning in this paper is a binary algorithm, the physical insights of each data point cannot fully account for the levels of the damage. A further study is required in advanced machine learning to build up a stronger correlation of data with the physical characteristics of a structure system.

The performance of the data-driven classification and the effects of damage levels on their effectiveness could be assessed by defining Type I and Type II errors (Figueiredo et al. 2011). Type I is defined as the false-positive classification, whereas the Type II is the false-negative one. From a system level, engineers could use the Type I error more than the Type II. Table 3 summarizes the number of Type I and Type II errors for each algorithm. In an overall analysis, different feature extraction methods and SNR show a trade-off between Type I and Type II errors; the THT-based algorithms are able to better detect damage (0.29 and 0.0%), and the HHT-based algorithms are able to better avoid Type II errors (0.0 and 0.0%).

Effects of Damage Location on Data Classification

To demonstrate the damage distribution over the span, six states (6, 8, and 10–13) were designed and organized to address the effects of damage locations under two different damage levels on data classification. The first set, States 6, 10, and 11, represents three damage locations at a quarter span, midspan, and three-quarter span, respectively, whereas the second set, States 8, 12, and 13, has a higher damage level of 40% cable stiffness reduction at the locations identical to the first set.

The results of the DIs of these scenarios are plotted in Figs. 9(a–f). Theoretically, the damaged location can lead to a change of frequency response. As a result, data exhibit a slightly higher variation due to different locations, particularly when exposed to different damage levels. A comparison of three different damage locations revealed that the data at the quarter span exhibited a scattered distribution that was sparser than the other two cases. Generally, the selected chirp excitation includes a wide frequency band; hence, it is capable of easily capturing the response of different states by using SVM learning.

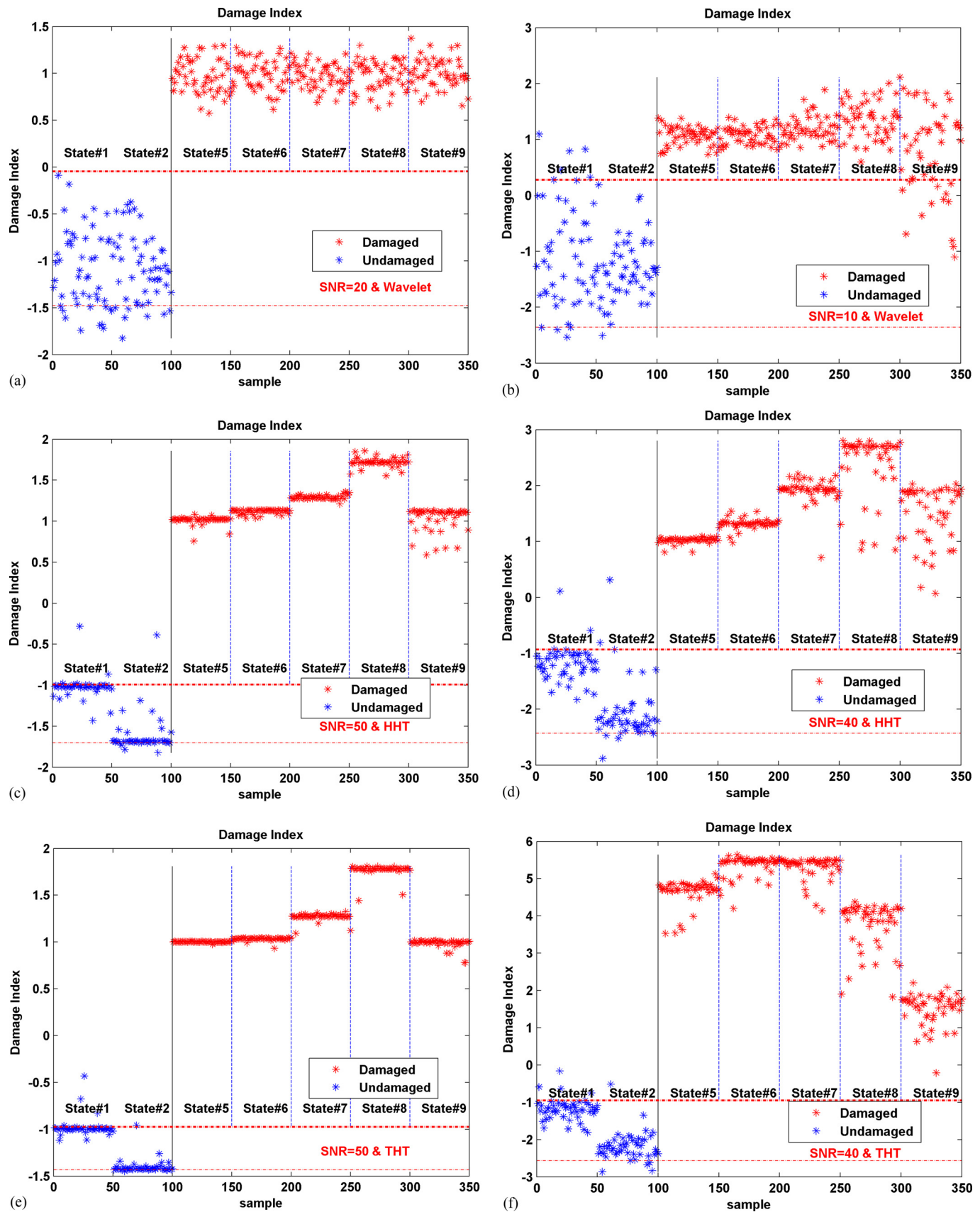


Fig. 8. (a–f) DIs from feature vectors under different damage levels

Table 3. Number and Percentage of Type I and Type II Errors

Algorithm	SNR	Error		
		Type I (%)	Type II (%)	Total (%)
Wavelet	10	5.33	3.20	4.57
	20	0.00	0.00	0.00
HHT	40	1.33	0.00	0.57
	50	0.00	0.00	0.00
THT	40	0.00	0.40	0.29
	50	0.00	0.00	0.00

Effects of Sensor Location on Data Classification

Another critical concern for the bridge engineering community is the sensor distribution. Reasonably, the closer the sensors are placed to the actual spots with damage/defects, the more sensitive the data could be for data identification. For a large-scale cable-stayed bridge, it is impossible to spatially distribute a large amount of sensor nodes to each location. As a result, the reduction of density of the sensor nodes could lead to missed readings of some damage-sensitive locations. Thus, this requires that the data captured from other locations are still capable of ensuring an effective data classification.

To demonstrate the effectiveness of the proposed data-driven methods and address the effects of the different sensor locations, three different locations were selected, from quarter-span, midspan, to three quarter-span, respectively, when subjected to the damage condition, as discussed in States 5–9. Figs. 10(a–c) plot the DIs of the results from three different sensor locations. Clearly, all cases exhibit a separable relation for the damage cases from the undamaged ones, regardless of the different locations, suggesting that the data classifiers could still maintain a higher prediction even at a location away from the damage spot. The reason behind this phenomenon is mainly because of the feature selection process. In this study, a feature selection method is used before the machine learning data process, whereas the trained features for all the cases are the highest separable data. Moreover, the ease in data classification is also due to the response of this study idealized from the numerical simulation. Consider that the actual data in the field could be easily contaminated by complex operational conditions, in which some dynamic information may disappear due to other localized interferences.

Effects of Moving Vehicle Load on Data Classification

Moving vehicles have been identified as excitation in the system identification and damage detection of the bridges (Zhang et al. 2012; Zhu and Law 2015). Moving vehicle loads can excite structural vibrations with large amplitudes and high SNRs (Zhang et al. 2012; Zhu and Law 2015). To discuss the effects of the moving vehicle on the data identification, States 14 and 15 were designed using the AASHTO HL-93 design truck with two speeds compared with the baselines at States 3 and 4 (AASHTO 2008). For simplicity, only the results using machine learning with the wavelet transform are presented. The major trends of the effectiveness by the other two methods should be identical to the early observations in the previous sections.

Bridge responses, including dynamic displacement, velocity, and acceleration at the midspan of the first span, are plotted in Fig. 11. Clearly, dynamic characteristics of the cable-stayed bridge under two speeds have no high variation. Also, from the point of view of their dynamic response caused by a vehicle, there is no clear separable relation between damaged and undamaged cases, as reported in the literature (Zhang et al. 2017). This is partially

because the reduction of single cable stiffness may not be sensitive to the dynamic response of the entire large-scale bridge.

Interestingly, the DIs of the results using SVM learning, illustrated in Figs. 12(a and b), revealed that the classifiers still have high performance to ensure the identification of damaged and undamaged cases, even under the noise level of 20 dB.

Conclusions

This study presented a time-frequency-based data-driven structural diagnosis and damage detection for large-scale cable-stayed bridges. Three representative feature extraction techniques were selected to enhance the feature extraction for sensor data, whereas the kernel function-based SVM was used to facilitate pattern recognition and improve the identification of damaged and undamaged cases. The time-frequency analysis revealed that different data-driven algorithms demonstrated respective advantages in different aspects. The developed strategy was finally illustrated through a case study. The ROC curves and AUC values were used as tools to quantify the accuracy of the optimization-based SVMs. A further parametric study was conducted to address some major concerns for practical applications in cable-stayed bridges. In summary, these conclusions can be drawn as follows:

1. The data-driven damage detection techniques exhibit high accuracy for distinguishing between undamaged and damaged cases, even when there are certain noise interferences and operational conditions.
2. The time-frequency analysis is effective for damage detection because the time-frequency analysis is more sensitive to damage, when the dynamics change from different states. In addition, the change of the dynamic characteristic of the cable-stayed bridges influences the time-frequency plane, providing more key information than just time or frequency domain. Accordingly, using data-driven machine learning can have a high classification accuracy in time series.
3. Selecting better damage features is key to yielding good damage classification for those complex data from large-scale cable-stayed bridges. Results have demonstrated the importance of the selection of damage feature techniques for damage detection. Clearly, the wavelet transform has a significantly higher accuracy in noise interference than that of the HTH and THT. The THT is the best algorithm for data analysis of regular signals, but for irregular signals it has a poor performance because it has higher sensitivity to local fluctuation. Furthermore, the ROC curves and value of the AUC further confirm that the wavelet transform behaves as a filter in the lower frequency part, leading to a higher reliable data identification when compared with the other two techniques.
4. Computation time is key for the data process, and this study shows that the THT and HHT are almost 10 times faster than the wavelet transform, which will be extremely important for processing the massive amounts of data captured from large-scale cable-stayed bridges in practice.
5. An extensive parametric study reveals that the data-driven classification could effectively address the major factors of interest, including the effects of damage level, damage location, sensor location, and moving load. The results in the THT and HHT methods exhibit clear discrimination between each damaged state, even under operational and environmental variability. The DIs of the results under moving vehicle revealed that the classifiers still have high performance to ensure the identification of damaged and undamaged cases, even under the noise level of 20 dB.

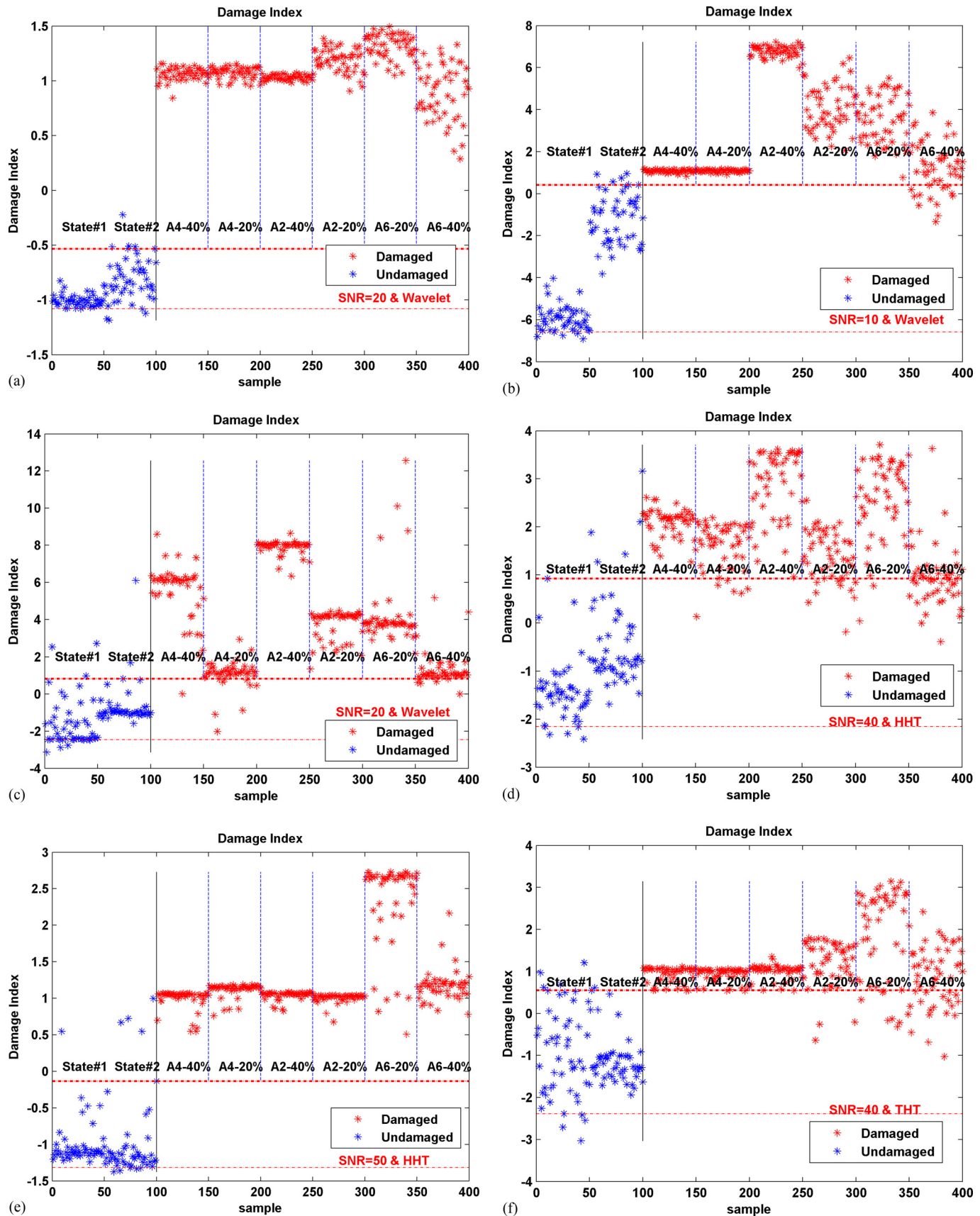


Fig. 9. (a–f) DIs from feature vectors under different damage locations

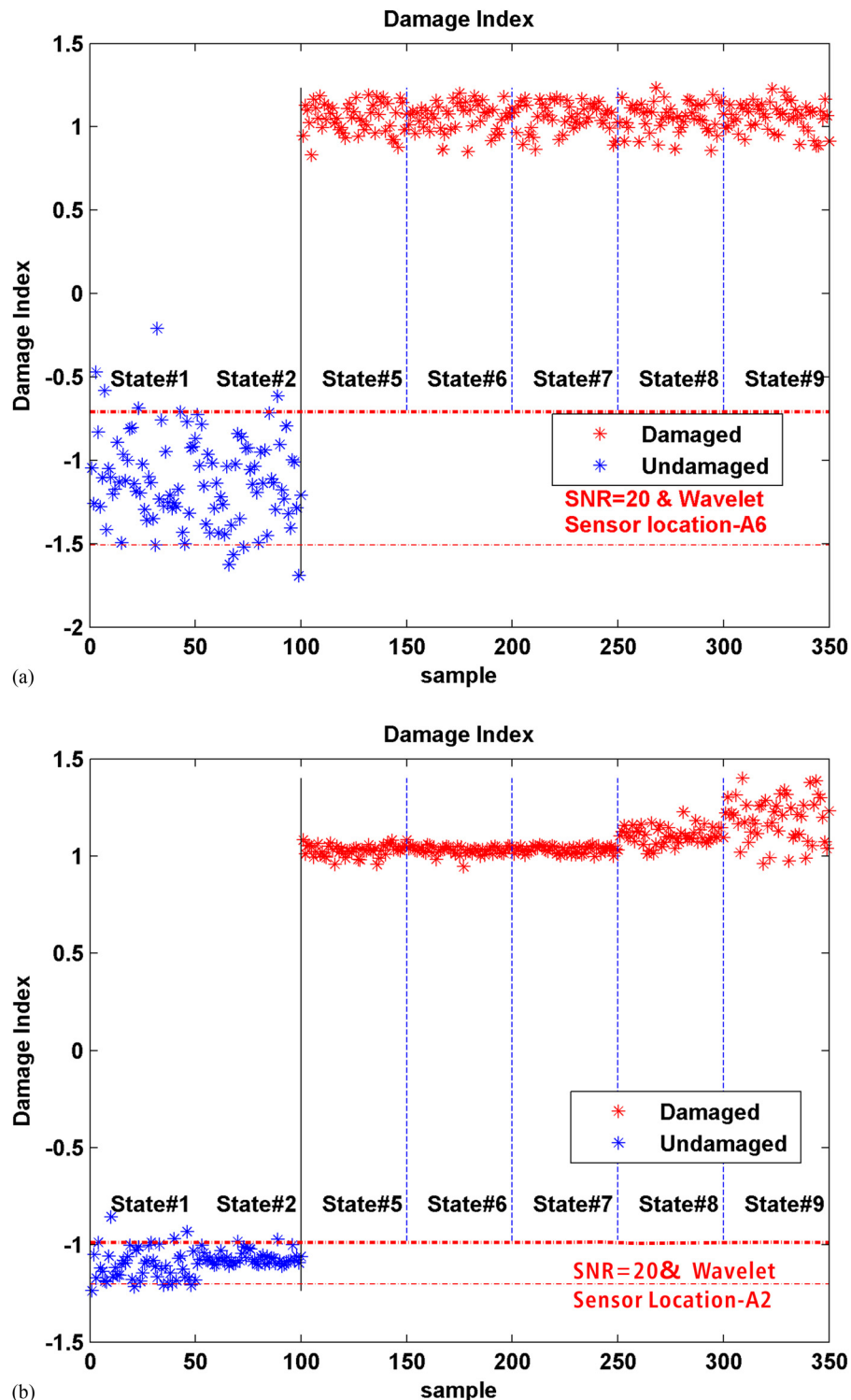


Fig. 10. (a–c) DIs from feature vectors under different sensor locations

- This study is based on the simulated data, and actual field data in the bridges could be more complex and could be contaminated by various operational and environmental variabilities. As such, any further investigation on the effectiveness and applicability of the proposed methods must be calibrated from training data. More sources of variability must be well characterized by the training data for the algorithms to accurately learn their characteristics on the system's response; thus, they

could help to distinguish the damage from the operational and environmental variabilities.

Acknowledgments

The authors gratefully acknowledge the financial support provided by Ozbun Economic Development Award, North Dakota DOT,

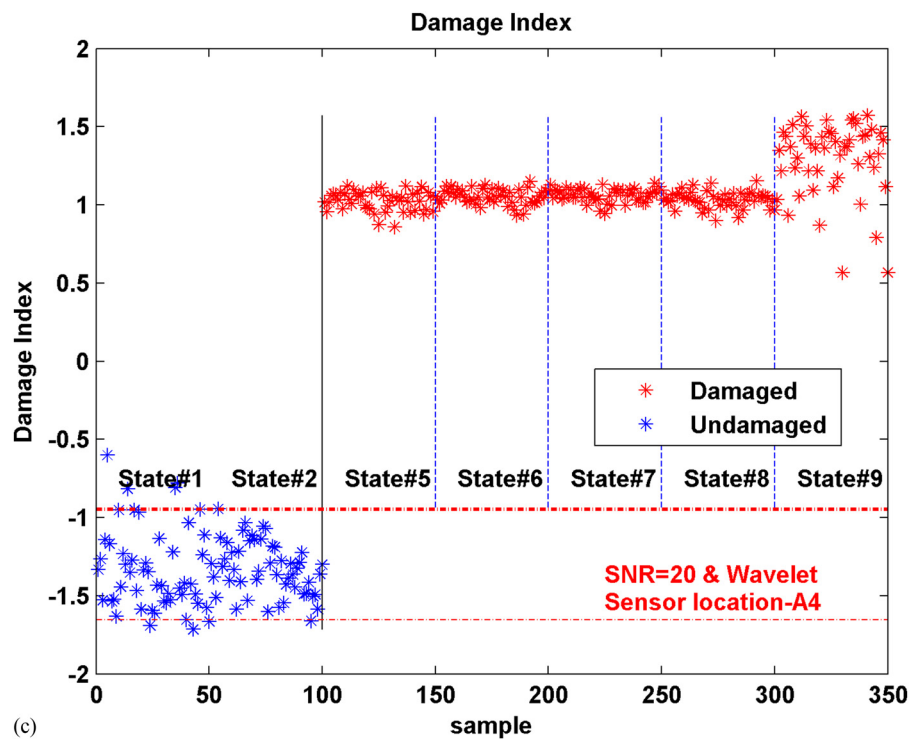


Fig. 10. (Continued.)

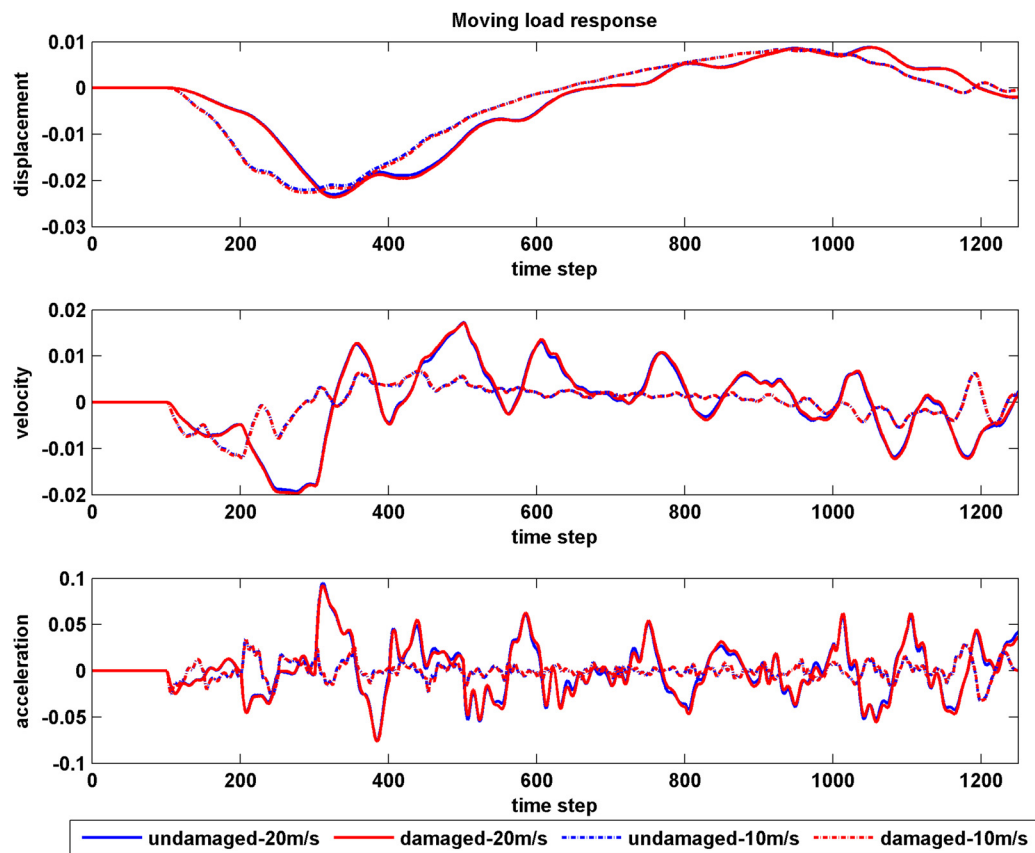


Fig. 11. Bridge dynamic responses under moving loads at two speeds

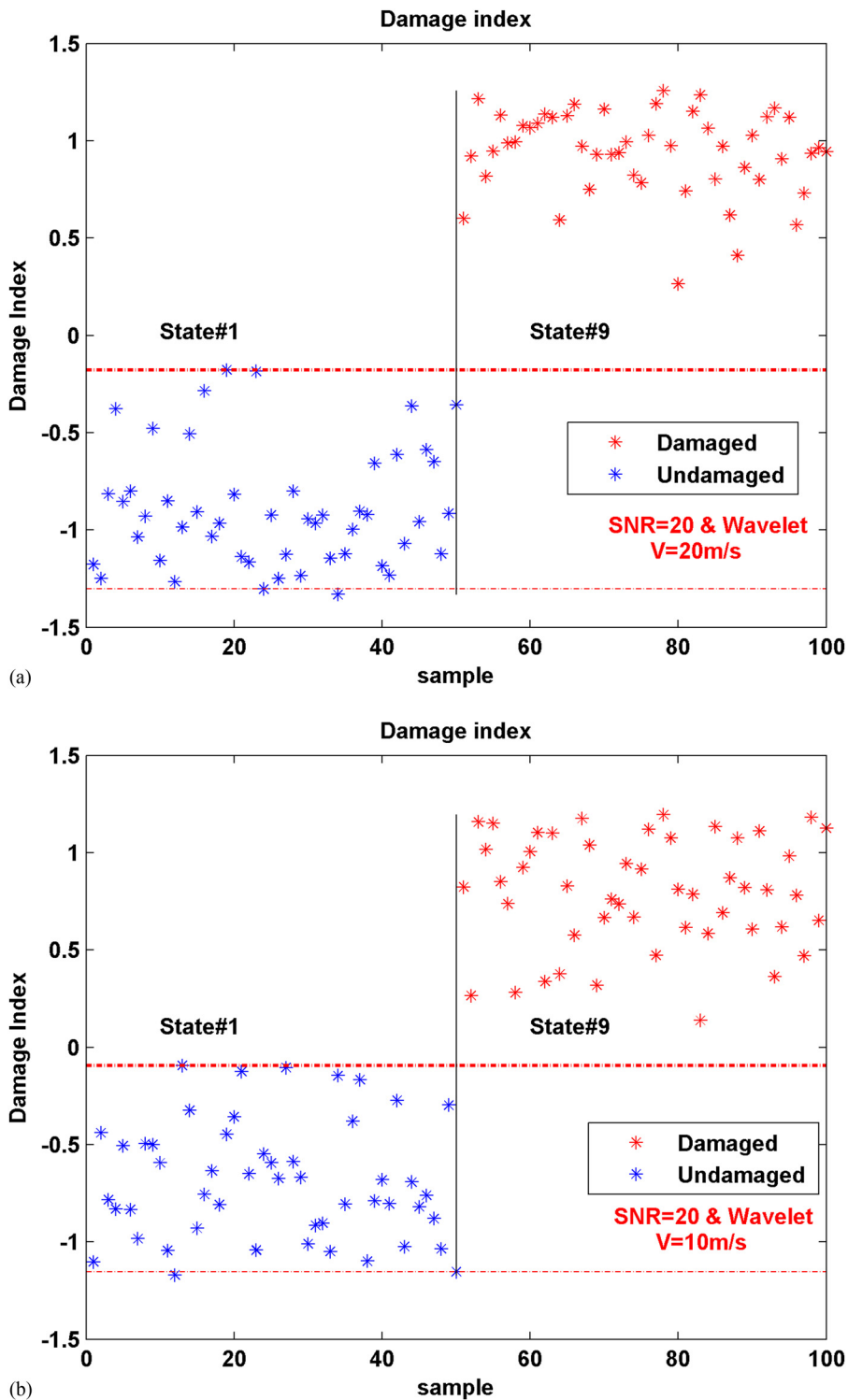


Fig. 12. (a and b) DIs for the cases of the wavelet transform under moving loads

U.S. DOT, and U.S. DOT CAAP Pipeline and Hazardous Materials. The results, discussion, and opinions reflected in this paper are those of the authors only and do not necessarily represent those of the sponsors.

Notation

The following symbols are used in this paper:

DI_i = i th damage index;

$\mathcal{F}\{\cdot\}$ = Fourier transform;

Fea_i = i th feature from the input data;

$Feature_i$ = i th resulting feature;

$H[h_{ik}(t)]$ = Hilbert transform;

$H(\omega, t)$ = Hilbert-Huang time-frequency spectrum;

$K(x, x_i)$ = kernel function;

$Label_i$ = i th support vector point from the training process;

P_{noise} = average power of noise;

P_{signal} = average power of signal;
 r_n = for which, no more IMFs can be extracted;
 $\text{TK}(t, f)$ = Teager-Kaiser spectrum;
 $Wx(a, b)$ = continues wavelet transform of the signal;
 w = vector that defines the position of the hyperplane;
 $w_i(t)$ = instantaneous frequency;
 $x(t)$ = original signal;
 y_i = training data coordinates;
 α_i = parameter of the hyperplane;
 ξ_i = measure of how much an observation fails to satisfy the target margin;
 ψ = basic function; and
 ψ^* = complex conjugate of the basic function, ψ .

References

- AASHTO. (2008). *LRFD HL-93 Loading*, Washington, DC.
- Atmaca, B., Yurdakul, M., and Ates, S. (2014). "Nonlinear dynamic analysis of base isolated cable-stayed bridge under earthquake excitations." *Soil Dyn. Earthquake Eng.*, 66(Nov), 314–318.
- Atmaca, B., Yurdakul, M., and Ates, S. (2015). "Dynamic behavior of cables of cable-stayed bridge isolated with SCFP placed under pylon." *Proc., 2015 World Congress on Advances in Structural Engineering And Mechanics*, Incheon, South Korea.
- Battista, R. C., Pfeil, M. S., and Carvalho, E. M. (2008). "Fatigue life estimates for a slender orthotropic steel deck." *J. Constr. Steel Res.*, 64(1), 134–143.
- Bin, G. F., Gao, J. J., Li, X. J., and Dhillon, B. S. (2012). "Early fault diagnosis of rotating machinery based on wavelet packets—Empirical mode decomposition feature extraction and neural network." *Mech. Syst. Signal Process.*, 27(Feb), 696–711.
- Bornn, L., Farrar, C. R., and Park, G. (2010). "Damage detection in initially nonlinear systems." *Int. J. Eng. Sci.*, 48(10), 909–920.
- Bouchikhi, A., Boudraa, A. O., Cexus, J. C., and Chonavel, T. (2014). "Analysis of multicomponent LFM signals by Teager Huang-Hough transform." *IEEE Trans. Aerosp. Electron. Syst.*, 50(2), 1222–1233.
- Cexus, J. C., and Boudraa, A. O. (2006). "Nonstationary signals analysis by Teager-Huang transform (THT)." *Proc., 14th European Signal Processing Conf.*, IEEE, Florence, Italy, 1–5.
- Cexus, J. C., Boudraa, A. O., and Bouchikhi, A. (2010). "A combined Teager-Huang and Hough transforms for LFM signals detection." *Proc., 2010 4th Int. Symp. on Communications, Control and Signal Processing (ISCCSP)*, IEEE, Piscataway, NJ, 1–5.
- Chinchalkar, S. (2001). "Determination of crack location in beams using natural frequencies." *J. Sound Vib.*, 247(3), 417–429.
- Comanducci, G., Magalhães, F., Ubertini, F., and Cunha, Á. (2016). "On vibration-based damage detection by multivariate statistical techniques: Application to a long-span arch bridge." *Struct. Health Monit.*, 15(5), 505–524.
- Daubechies, I. (1990). "The wavelet transform, time-frequency localization and signal analysis." *IEEE Trans. Inf. Theory*, 36(5), 961–1005.
- Doebling, S. W., Farrar, C. R., and Prime, M. B. (1998). "A summary review of vibration-based damage identification methods." *Shock Vib. Digest*, 30(2), 91–105.
- Fahim, A. A., Gallego, R., Bochud, N., and Rus, G. (2013). "Model-based damage reconstruction in composites from ultrasound transmission." *Composites Part B*, 45(1), 50–62.
- Fan, J., Upadhye, S., and Worster, A. (2006). "Understanding receiver operating characteristic (ROC) curves." *Can. J. Emergency Med.*, 8(1), 19–20.
- Farrar, C. R., and Worden, K. (2013). *Structural health monitoring: A machine learning perspective*, John Wiley & Sons, Chichester, U.K.
- Fasl, J. D. (2013). "Estimating the remaining fatigue life of steel bridges using field measurements." Ph.D. dissertation, Univ. of Texas at Austin, Austin, TX.
- Feng, Z., Liang, M., and Chu, F. (2013). "Recent advances in time-frequency analysis methods for machinery fault diagnosis: A review with application examples." *Mech. Syst. Signal Process.*, 38(1), 165–205.
- Figueiredo, E., Park, G., Farrar, C. R., Worden, K., and Figueiras, J. (2011). "Machine learning algorithms for damage detection under operational and environmental variability." *Struct. Health Monit.*, 10, 559–572.
- Flandrin, P., Rilling, G., and Goncalves, P. (2004). "Empirical mode decomposition as a filter bank." *IEEE Signal Process. Lett.*, 11(2), 112–114.
- Ge, R., Pan, H., Lin, Z., Gong, N., and Wang, J. (2016). "RF-powered battery-less wireless sensor network." *Proc., 5th Int. Symp. on Next-Generation Electronics*, Hsinchu, Taiwan, 32–33.
- Ge, Y., and Xiang, H. (2011). "Concept and requirements of sustainable development in bridge engineering." *Front. Archit. Civil Eng. China*, 5(4), 432–450.
- Gerist, S., and Maher, M. R. (2016). "Multi-stage approach for structural damage detection problem using basis pursuit and particle swarm optimization." *J. Sound Vib.*, 384(Dec), 210–226.
- Gui, G., Pan, H., Lin, Z., Li, Y., and Yuan, Z. (2017). "Data-driven support vector machine with optimization techniques for structural health monitoring and damage detection." *KSCJ. Civ. Eng.*, 21(2), 523–534.
- Guo, T., Liu, Z., and Zhu, J. (2015). "Fatigue reliability assessment of orthotropic steel bridge decks based on probabilistic multi-scale finite element analysis." *Adv. Steel Constr.*, 11(3), 334–346.
- Herrasti, Z., Val, I., Gabilondo, I., Berganzo, J., Arriola, A., and Martínez, F. (2016). "Wireless sensor nodes for generic signal conditioning: Application to structural health monitoring of wind turbines." *Sens. Actuators A*, 247(Aug), 604–613.
- Hou, Z., Noori, M., and Amand, R. S. (2000). "Wavelet-based approach for structural damage detection." *J. Eng. Mech.*, 10.1061/(ASCE)0733-9399(2000)126:7(677), 677–683.
- Hsu, W.-K., Chiou, D.-J., Chen, C.-W., Liu, M.-Y., Chiang, W.-L., and Huang, P.-C. (2013). "RETRACTED: Sensitivity of initial damage detection for steel structures using the Hilbert-Huang transform method." *J. Vib. Control*, 19(6), 857–878.
- Huang, N. E., et al. (1971). "The empirical mode decomposition and the Hilbert spectrum for nonlinear and non-stationary time series analysis." *Proc. R. Soc. London, Ser. A*, 454(1971), 903–995.
- Huang, Q., Tang, B., and Deng, L. (2015). "Development of high synchronous acquisition accuracy wireless sensor network for machine vibration monitoring." *Measurement*, 66(Apr), 35–44.
- Jang, J. (2016). "Development of data analytics and modeling tools for civil infrastructure condition monitoring applications." Ph.D. dissertation, Columbia Univ., New York.
- Junsheng, C., Dejie, Y., and Yu, Y. (2007). "The application of energy operator demodulation approach based on EMD in machinery fault diagnosis." *Mech. Syst. Signal Process.*, 21(2), 668–677.
- Kim, H., and Melhem, H. (2004). "Damage detection of structures by wavelet analysis." *Eng. Struct.*, 26(3), 347–362.
- Ko, J. M., and Ni, Y. Q. (2005). "Technology developments in structural health monitoring of large-scale bridges." *Eng. Struct.*, 27(12), 1715–1725.
- Kopsaftopoulos, F. P., and Fassois, S. D. (2013). "A functional model based statistical time series method for vibration based damage detection, localization, and magnitude estimation." *Mech. Syst. Signal Process.*, 39(1–2), 143–161.
- Lee, J. (2009). "Identification of multiple cracks using natural frequencies." *J. Sound. Vib.*, 320(3), 482–490.
- Li, H., and Ou, J. (2016). "The state of the art in structural health monitoring of cable-stayed bridges." *J. Civ. Struct. Health Monit.*, 6(1), 43–67.
- Li, H., Zhang, Y., and Zheng, H. (2010). "Bearing fault detection and diagnosis based on order tracking and Teager-Huang transform." *J. Mech. Sci. Technol.*, 24(3), 811–822.
- Li, H., Zheng, H., and Tang, L. (2009). "Bearing fault detection and diagnosis based on Teager–Huang transform." *Int. J. Wavelets Multiresolution Inf. Process.*, 7(5), 643–663.

- Li, H., Zheng, H., and Tang, L. (2010). "Gear fault detection based on Teager-Huang transform." *Int. J. Rotating Mach.*, 502064.
- Lin, J., and Qu, L. (2000). "Feature extraction based on Morlet wavelet and its application for mechanical fault diagnosis." *J. Sound Vib.*, 234(1), 135–148.
- Lin, Z., Fakharifar, M., Huang, Y., Chen, G., and Wang, Z. (2014). "Damage detection of a full-size concrete box girder bridge with the moving-window least-square fitting method." *Proc., NDE/NDT for Structural Materials Technology for Highway & Bridges*, American Society for Nondestructive Testing, Columbus, OH.
- Magalhães, F., Cunha, A., and Caetano, E. (2012). "Vibration based structural health monitoring of an arch bridge: From automated OMA to damage detection." *Mech. Syst. Signal Process.*, 28(Apr), 212–228.
- Maljaars, J., van Dooren, F., and Kolstein, H. (2012). "Fatigue assessment for deck plates in orthotropic bridge decks." *Steel Constr.*, 5(2), 93–100.
- Mandic, D. P., Rehman, N. U., Wu, Z., and Huang, N. E. (2013). "Empirical mode decomposition-based time-frequency analysis of multivariate signals: The power of adaptive data analysis." *IEEE Signal Process. Mag.*, 30(6), 74–86.
- Masciotta, M. G., Ramos, L. F., Lourenço, P. B., and Vasta, M. (2014). "Damage detection on the Z24 bridge by a spectral-based dynamic identification technique." *Dynamics of civil structures*, F. Catbas, ed., 4, Springer, Cham, Switzerland, 197–206.
- Masri, S., Smyth, A., Chassiakos, A., Caughey, T., and Hunter, N. (2000). "Application of neural networks for detection of changes in nonlinear systems." *J. Eng. Mech.*, 10.1061/(ASCE)0733-9399(2000)126:7(666), 666–676.
- MATLAB [Computer software]. MathWorks, Natick, MA.
- Oh, C. K., and Sohn, H. (2008). "Unsupervised support vector machine based principal component analysis for structural health monitoring." *ICCES*, 8(3), 91–99.
- Oh, C. K., and Sohn, H. (2009). "Damage diagnosis under environmental and operational variations using unsupervised support vector machine." *J. Sound Vib.*, 325(1–2), 224–239.
- Pakrashi, V., Basu, B., and O'Connor, A. (2007). "Structural damage detection and calibration using wavelet-kurtosis technique." *Eng. Struct.*, 29(9), 2097–2108.
- Pan, H., Azimi, M., Gui, G., Yan, F., and Lin, Z. (2018). "Vibration-based support vector machine for structural health monitoring." *Proc., 7th Int. Conf. on Experimental Vibration Analysis for Civil Engineering Structures*, J. Conte, R. Astroza, G. Benzon, G. Feltrin, K. Loh, and B. Moaveni, eds., 5, Springer, Cham, Switzerland.
- Pan, H., Ge, R., Wang, J., Gong, N., and Lin, Z. (2016). "Integrated wireless sensor networks with UAS for damage detection and monitoring of bridges and other large-scale critical civil infrastructures." *Proc., NDE/NDT for Highway and Bridges: Structural Materials Technology*, American Society for Nondestructive Testing, Columbus, OH.
- Pavlopoulou, S., Worden, K., and Soutis, C. (2016). "Novelty detection and dimension reduction via guided ultrasonic waves: Damage monitoring of scarf repairs in composite laminates." *J. Intell. Mater. Syst. Struct.*, 27(4), 549–566.
- Rashedi, R., and Hegazy, T. (2015). "Capital renewal optimisation for large-scale infrastructure networks: Genetic algorithms versus advanced mathematical tools." *Struct. Infrastruct. Eng.*, 11(3), 253–262.
- Salawu, O. S. (1997). "Detection of structural damage through changes in frequency: A review." *Eng. Struct.*, 19(9), 718–723.
- SAP2000 [Computer software]. Computers & Structures, Inc., Walnut Creek, CA.
- Silva, M., Santos, A., Figueiredo, E., Santos, R., Sales, C., and Costa, J. C. W. A. (2016). "A novel unsupervised approach based on a genetic algorithm for structural damage detection in bridges." *Eng. App. Artif. Intell.*, 52(Jun) 168–180.
- Simonovski, I., and Bolte, M. (2003). "Damping identification using a continuous wavelet transform: Application to real data." *J. Sound Vib.*, 262(2), 291–307.
- Sun, Z., and Chang, C. (2002). "Structural damage assessment based on wavelet packet transform." *J. Struct. Eng.*, 10.1061/(ASCE)0733-9445(2002)128:10(1354), 1354–1361.
- Wang, Z. C., and Chen, G. D. (2013). "A moving-window least squares fitting method for crack detection and rigidity identification of multispan bridges." *Struct. Control Health Monit.*, 20(3), 387–404.
- Watters, D. G., Jayaweera, P., Bahr, A. J., and Huestis, D. L. (2002). "Design and performance of wireless sensors for structural health monitoring." *Proc., Review of Progress in Quantitative Nondestructive Evaluation*, 615, American Institute of Physics, Melville, NY, 969–976.
- Worden, K., Farrar, C. R., Manson, G., and Park, G. (2007). "The fundamental axioms of structural health monitoring." *Proc. R. Soc. London, Ser. A*, 463(2082), 1639–1664.
- Xia, Y., Nassif, H., Hwang, E.-S., and Linzell, D. (2013). "Optimization of design details in orthotropic steel decks subjected to static and fatigue loads." *Transportation Research Record* 2331, 14–23.
- Yan, F., Chen, W., and Lin, Z. (2016). "Prediction of fatigue life of welded details in cable-stayed orthotropic steel deck bridges." *Eng. Struct.*, 127(Nov), 344–358.
- Yan, F., Lin, Z., and Huang, Y. (2017). "Numerical simulation of fatigue behavior for cable-stayed orthotropic steel deck bridges using mixed-dimensional coupling method." *KSCE J. Civ. Eng.*, 21(6) 2238–2350.
- Yan, R., Gao, R., and Chen, X. (2014). "Wavelet for fault diagnosis of rotary machines: A review." *Signal Process.*, 96(Mar) 1–15.
- Yang, J., Lei, Y., Lin, S., and Huang, N. (2004). "Hilbert-Huang based approach for structural damage detection." *J. Eng. Mech.*, 10.1061/(ASCE)0733-9399(2004)130:1(85), 85–95.
- Yu, D., Cheng, J., and Yang, Y. (2005). "Application of EMD method and Hilbert spectrum to the fault diagnosis of roller bearings." *Mech. Syst. Signal Process.*, 19(2), 259–270.
- Zang, C., and Imregun, M. (2001). "Structural damage detection using artificial neural networks and measured FRF data reduced via principal component projection." *J. Sound Vib.*, 242(5), 813–827.
- Zhang, W., Li, J., Hao, H., and Ma, H. (2017). "Damage detection in bridge structures under moving loads with phase trajectory change of multi-type vibration measurements." *Mech. Syst. Signal Process.*, 87(Mar), 410–425.
- Zhang, Y., Wang, L. Q., and Xiang, Z. H. (2012). "Damage detection by mode shape squares extracted from a passing vehicle." *J. Sound Vib.*, 331(2), 291–307.
- Zhu, X. Q., and Law, S. S. (2015). "Structural health monitoring based on vehicle-bridge interaction: Accomplishments and challenges." *Adv. Struct. Eng.*, 18(12), 1999–2015.
- Zou, Y., Tong, L., and Steven, G. P. (2000). "Vibration-based model-dependent damage (delamination) identification and health monitoring for composite structures—A review." *J. Sound Vib.*, 230(2), 357–378.